

# Model Independent Bounds on the Non-Oscillatory Explanations of the MiniBooNE Excess

Vedran Brdar,<sup>a</sup> Oliver Fischer,<sup>b</sup> and Alexei Yu. Smirnov<sup>c</sup>

*Max-Planck-Institut für Kernphysik, 69117 Heidelberg, Germany*

We consider the non-oscillatory explanations of the low energy excess of events detected by MiniBooNE. We present a systematic search for phenomenological scenarios based on new physics which can produce the excess. We define scenarios as series of transitions and processes which connect interactions of accelerated protons on target with single shower events in the MiniBooNE detector. The key elements of the scenarios are production and decay of new light  $\mathcal{O}(\text{keV} - 100 \text{ MeV})$  particles (fermions or/and bosons). We find about 20 scenarios with minimal possible number of new particles and interaction points. In practice, they are all reduced to few generic scenarios and in this sense and in this way we develop the effective theory of the MiniBooNE excess. We consider tests of these scenarios with near or close detectors in neutrino experiments T2K ND280, NO $\nu$ A, MINER $\nu$ A as well as in NOMAD and PS191. The scenarios allow to immediately connect the MiniBooNE excess and the expected number of new physics events in these detectors. We compute the expected number of events in these detectors as functions of lifetimes and masses of new particles and confront them with the corresponding experimental bounds. We show that practically all scenarios are excluded or strongly disfavored by one or several experiments.

## I. INTRODUCTION

The jury is still out on whether the new physics effects are necessary for explanation of the low energy excess of  $e$ -like events observed by MiniBooNE [1, 2]. In this work we assume that the answer to this question is affirmative. The popular explanation based on oscillations driven by mixing with new eV-scale neutrino is very strongly disfavored, if not excluded<sup>1</sup>. Not only global neutrino oscillation fit [4] but also properties of the excess (energy and angular distributions) are behind the last statement.

In this connection various non-oscillatory explanations of the excess were proposed. Most of them make use of possible misidentification of the MiniBooNE events which can be due to electrons, photons, unresolved  $e^+e^-$ , and  $\gamma\gamma$  pairs. The explanations are based on production and decay of new heavy neutrinos or bosons with mass in the  $\mathcal{O}(\text{keV} - 100 \text{ MeV})$  range and include:

- Production of  $N$  in the detector via  $\nu_\mu$  upscattering and then radiative  $N$ -decay [5];
- Production of  $N$  via mixing in  $\nu_\mu$  in the decay pipe and further radiative decay along the beamline and mainly in the detector [6];
- $N$  production in the detector via  $\nu_\mu$ -upscattering and decay with appearance of the  $e^+e^-$  pair. Two versions have been proposed: 3 body decay  $N \rightarrow \nu e^+e^-$  [7, 8], and two body decay  $N \rightarrow \nu B$ , followed by the decay of an on-shell boson  $B \rightarrow e^+e^-$ . Here  $B$  can be a new gauge boson  $Z'$  [9] or scalar  $B = S$  [10–12]. In these models,  $B$  has a decay length which is much smaller than the size of the detector,  $\lambda_B \ll d^{MB}$ , so that the event looks as local

<sup>a</sup> vbrdar@mpi-hd.mpg.de

<sup>b</sup> oliver.fischer@mpi-hd.mpg.de

<sup>c</sup> smirnov@mpi-hd.mpg.de

<sup>1</sup> An alternative oscillation scenario was discussed in ref. [3] where short baseline oscillations are due to very strong medium potential resonantly produced by scattering of neutrinos on relic neutrino background via a light neutrino-philic scalar boson. This explanation requires an enormous over-density of the local neutrino background.

decay of  $N$ . There is, however, an important kinematical difference to the 3-body decay of [7] since the invariant mass of the pair  $e^+e^-$  is determined by the mass of  $B$  which is smaller than the mass of  $N$ .

- $N$  production via mixing in the decay pipe and then decay  $N \rightarrow \nu_e \phi$  along the baseline with emission of  $\nu_e$  which then produces electron via CCQE scattering in the detector [13–15].
- Production of the light scalar  $B$  in upscattering of  $\nu_\mu$ ,  $\nu_\mu A \rightarrow n B A'$ , which then decays as  $B \rightarrow e^+ e^-$  [12]. (In the model  $B$  is produced via coupling with gauge boson mediator of the upscattering process.) The new neutrino  $n$  does not contribute to the MiniBooNE signal in contrast to the previous mechanisms.

It should be mentioned that these explanations do not provide a perfect fit to the MiniBooNE excess, they are disfavored by some other data, and most of them do not reproduce the LSND result (in contrast to oscillations). In particular, recent measurements of the bunch timing [2] do not show significant deviation (shift or widening) of the time distribution of the events from the one expected from usual light neutrinos [2]. This essentially excludes mechanisms of decay of heavy neutrinos in the second item and restricts parameters of the mechanism in item 1.

Do other possibilities of this type exist or is everything already covered (exhausted)? In this connection, we perform a systematic search of all possible phenomenological scenarios that can explain the MiniBooNE excess. We identify the simplest scenarios with a minimal number of new particles and new interaction vertices (points). Clearly, an increase of these points would introduce additional smallness since there are various restrictions on new interactions.

The goal of this paper is to perform model independent tests of explanations of the MiniBooNE excess. For this, we introduce scenarios, that is, sets of transitions and processes which connect proton interactions on target with the appearance of 1 shower events in MiniBooNE. We will use data from accelerator neutrino experiments with near or relatively close detectors. The scenarios allow us to directly connect number of events in detectors with the MiniBooNE excess. Various model dependent features simply cancel in this consideration. We describe these scenarios by a small number of parameters. The scenarios can be further (and even more strongly) restricted by other observations. For the introduced scenarios we compute the expected numbers of events in the near detector experiments and confront them with the experimental bounds.

The paper is organized as follows. In Section II we present a systematic search for the simplest phenomenological scenarios which allow to explain the MiniBooNE excess. We show that, in relevant aspects, they are reduced to just few qualitatively different possibilities (generic scenarios). In Section III we present general formulas for the number of events in the detectors as functions of parameters of the experimental setups and parameters of the scenarios which mainly include the lifetimes and masses of new particles. In Section IV, we present required parameters of employed experiments and derive experimental upper bounds on the number of events due to new physics. In Section V we compute expected number of events due to new physics in different scenarios and confront them with experimental bounds. Discussion and conclusions follow in Section VI.

## II. SCENARIOS FOR THE MINIBOONE EXCESS

### A. General bounds on explanations of the excess

MiniBooNE observed the excess of  $1sh-$  events of  $560.6 \pm 119.6$  and  $77.4 \pm 28.5$  in the neutrino and antineutrino mode (horn polarities), respectively [1]. The collected data corresponds to  $18.75 \times 10^{20}$  POT ( $11.27 \times 10^{20}$  POT) in neutrino (antineutrino) mode.

We will use the sum of the excesses:

$$N_{1sh}^{MB} = 638.0 \pm 132.8. \quad (1)$$

We assume that this excess is due to new physics and not due to underestimated or missed background as well as not due to oscillations related to existence of the eV-scale sterile neutrino.

The source of events are 8 GeV protons from Booster that hit the Beryllium target producing secondary particles. The 818 ton liquid scintillation detector observes via the Cherenkov radiation the single shower,  $1sh$ , events

$$p + A [target] \rightarrow [X] \rightarrow 1sh \text{ events } [detector]. \quad (2)$$

The recoiling nucleon can produce scintillation light, this additional source of light was not considered in the MB reconstruction<sup>2</sup>. The MiniBooNE detector is not capable to identify particle(s) which induce these EM showers.

The appearance of  $1sh$  events is time correlated with  $pA$  collisions in the target. Therefore, it should be a mediator(s) system  $X$  which connects the ends: the  $pA$ – interaction in the target and the EM shower in the detector. Furthermore, the arrival time distribution of events is consistent with the arrival time of the usual neutrinos. We will not discuss the LSND result: the requirement of joint a explanation imposes additional restrictions on scenarios.

What is the “black box”  $X$  in Eq. (2)? It can be production and propagation of new particles, or some new dynamics related to known particles like Lorentz violation [16], non-standard decoherence [17], *etc.* We will assume that the mediator system is some new particle (or system of particles)  $X_s$  that is produced in the source, evolves (in general, via a chain of processes),  $X_s \rightarrow X_{det}$ , and then interacts or decays in the detector,  $X_{det}$ , producing  $1sh$  events:

$$p + A [target] \rightarrow X_s [ \rightarrow ] X_{det} \rightarrow 1sh [detector]. \quad (3)$$

There are certain observations that eliminate many possibilities and allow us to make first step toward connecting “the ends”:

1. The proton beam energy,  $E \sim 8$  GeV, restricts the mass scale of new particles to be at most around few GeV. Since charged particles at this mass scale are excluded, the new particles should be electrically neutral.

2. Number of events in the excess with respect to the one of  $\nu_\mu$  and  $\nu_e$  CC events reads

$$\frac{N_{1sh}^{MB}}{N_\mu^{MB}} \simeq 10^{-2}, \quad \frac{N_{1sh}^{MB}}{N_e^{MB}} = 0.53. \quad (4)$$

Therefore, the processes which lead to the excess should not be rare (the yield should be comparable with the yield of usual neutrinos unless we assume that  $X$  has strong interaction).

3. The excess disappears in the beam dump run [18]: In this run roughly 30 events should have been produced but no excess was observed.

4. Comparison of the excess in  $\nu$  and  $\bar{\nu}$  modes (horn polarities).

*The implications of these results follow:*

**From the source side:** In general,  $X_s$  can be produced

---

<sup>2</sup> Being included in the analysis, the information on the recoil can help excluding various explanations and distinguish between the decay explanations and upscattering.

- on target in  $pA$  collisions immediately,
- in decays (interactions) of known particles produced in the  $pA$ -collisions, such as  $\pi$ ,  $K$ , heavy mesons,
- by usual neutrinos  $\nu_\mu$  in detector or/and surrounding matter along the baseline.

The beam-dump mode results and  $\nu - \bar{\nu}$  results exclude the first possibility. The number of excess events in  $\nu$  and  $\bar{\nu}$  modes corresponds to what is expected for usual neutrinos which implies the same production difference and the same interaction for  $X$ . Neutral particle decays as sources of  $X_s$  are excluded since they are not affected by the magnetic field and beam-dump [19]. Thus, we arrive at the conclusion that  $X_s$  should be produced in the charged  $\pi$ ,  $K$  decays immediately or by neutrinos produced in these decays.

**From the detector side:** the  $1sh$  MiniBooNE events can be produced by  $e$ ,  $\gamma$ , collimated  $e^+e^-$  pair and collimated  $\gamma\gamma$ , that is, by state  $\xi$

$$\xi = e, \gamma, e^+e^-, \gamma\gamma. \quad (5)$$

We will not consider more complicated systems, since their production will bring additional suppression. Fluxes of particles  $\xi$  from the outside are suppressed by absorption in walls, rejection by anticoincidence system and fiducial volume cut. Furthermore, radial distribution of events shows that the excess increases toward the center [2]. Therefore,  $X_{det}$  in (3) should be some neutral particle that enters MiniBooNE and produces  $\xi$  in interaction or decay inside the detector.

The particle(s)  $X_{det}$  (as well as  $X_s$ ) can be fermion  $N$  or boson  $B$ , and the latter can be scalar or vector bosons. For fermions, we consider spin 1/2 although spin 3/2 like gravitino can also be considered. For definiteness we will mainly explore spin 1/2 fermion and boson cases,  $X = N, B$ . We will consider separately the cases with bosons which show some qualitatively new features.

If  $X_s = N$  – a new heavy neutrino – it can be produced via mixing with  $\nu_\mu$ . Therefore, the relevant channels of production are the same as for  $\nu_\mu$  with substitution  $\nu_\mu \rightarrow N$ . If  $X_s = B$ , the decays are the same as the standard decay modes of  $K$  and  $\pi$  with additional  $B$  emission (bremsstrahlung)  $K \rightarrow \mu\nu B$ ,  $\pi \rightarrow \mu\nu B$ , or standard modes in which one of pions is substituted by  $B$ :  $K \rightarrow \pi B$ ,  $K \rightarrow \pi\pi B$ . Details of these decays, values of couplings, bounds etc. are not important for our analysis.

Moving further, the electromagnetic systems (5) can be produced in decays of  $N$  or in interactions. Due to fermionic nature, the  $N$ -decays can proceed with the usual neutrinos or with a new neutral fermion  $N'$ :

$$N \rightarrow \nu + \xi, \quad N \rightarrow N' + \xi. \quad (6)$$

The simplest possibilities include the radiative decay ( $\xi = \gamma$ ):

$$N \rightarrow \nu + \gamma, \quad (7)$$

and 3 body decay ( $\xi = e^+e^-$ )

$$N \rightarrow \nu + e^+ + e^-, \quad (8)$$

or decay via production of on-shell boson (double decay):

$$N \rightarrow \nu + B, \quad B \rightarrow e^+ + e^- \text{ or } B \rightarrow \gamma + \gamma. \quad (9)$$

Here,  $B$  can be  $\pi^0$  or some new scalar or vector boson.

Alternatively,  $\xi$  can be produced in  $N$ -interactions with electrons or nucleons (A):

$$N + e \rightarrow e + N', \quad N + A \rightarrow e + A', \quad (10)$$

where  $N$  can coincide with the usual neutrinos  $\nu_\mu$  or  $\nu_e$ .

In the case of new bosonic particles,  $X_{det} = B$ , the state  $\xi$  can be produced in the 2-body decays:

$$B \rightarrow e^+ + e^-, \quad B \rightarrow \gamma + \gamma, \quad B \rightarrow B' + \gamma, \quad (11)$$

or 3 body decay

$$B \rightarrow B' + e^+ + e^-. \quad (12)$$

Also,  $\xi$  can appear in interactions with detector nuclei and electrons:

$$B + A \rightarrow A + e^+ + e^-, \quad B + A \rightarrow A + \gamma, \quad B + e \rightarrow B + e. \quad (13)$$

## B. Combinatorics of connections. Scenarios.

Let us consider all possible connections of the source and detector parts, *i.e.* transformation  $X_s \rightarrow X_{det}$ . In the simplest case,  $X_s$  and  $X_{det}$  coincide,  $X_s = X_{det}$ . The next possibility is that  $X_{det}$  is produced in decays of  $X_s$  or in interactions of  $X_s$  with the medium on the way to a detector (or inside detector itself). Several particles can be involved via a chain of processes connecting the ends:  $X_s \rightarrow X_1 \rightarrow X_2 \dots \rightarrow X_{det}$ . At this point, we will employ criteria of minimality: we identify the simplest links with minimal number of chains or interactions points. Notice that, in general, any new vertex or additional new particle typically brings an additional suppression and it is difficult to produce the required number of events in MiniBooNE.

Let us consider transitions with two and more number of interaction points which include production and decay of a new fermion  $N$  or boson  $B$ <sup>3</sup>.

Heavy neutrino  $N$  can be produced:

- in decays of usual mesons  $\pi$  and  $K$  in a decay pipe (for  $N$  it is due to mixing with usual neutrinos). We call this element M - mixing.
- by the  $\nu_\mu$  interactions with matter outside the pipe. That is, the  $U_\nu$ - upscattering.

Difference of these two possibilities is that, in the  $M$ -case,  $N$  is produced via mixing with  $\nu_\mu$ , while in the latter case – in the  $\nu_\mu$  interaction. Furthermore, in the  $M$ -case the  $N$ -flux is formed in the decay pipe, while in  $U_\nu$ -case  $N$  are produced outside the decay pipe.

In turn,  $N$  can decay

- immediately into  $\xi$  ( $D_\xi$ );

---

<sup>3</sup> Notice that the simplest scenario would be with single non-standard interactions vertex, when  $X_s = X_{det} = \nu_\mu$ . Now,  $\nu_\mu$ , from standard  $\pi$  and  $K$  decays, produce electrons in the detector via the charged current non-standard interaction (CC NSI)  $\nu_\mu + A \rightarrow e + A'$  (This implies that  $\nu_\mu$  is not orthogonal to  $\nu_e$ ) or via neutral current (NC) NSI on electrons. Such a possibility is restricted very strongly.

- into a state with  $\nu_e$ , which then produces  $\xi = e$  interacting in the detector ( $D_\nu$ );
- into new neutral particles  $N \rightarrow B$  which then decay into  $\xi$  ( $D_B D_\xi$ ).

Instead of decay,  $N$  can upscatter on nucleons and electrons in the detector (and outside the detector, in the dirt) to produce  $\xi$  ( $U_\xi$ ). But this would involve another smallness due to additional non-standard interaction. Indeed, the probability of  $N$  interactions equals  $P_N = \sigma_N n l$ , where  $n$  is the number density of scatterers and  $l$  is the length of trajectory along which  $N$  interacts. For new 4-fermion interactions characterized by coupling  $G_N$  we obtain

$$P_N = 5 \cdot 10^{-11} \left( \frac{l}{10\text{m}} \right) \left( \frac{n}{3n_A} \right) \left( \frac{E_N}{1 \text{ GeV}} \right) \left( \frac{G_N}{G_F} \right)^2, \quad (14)$$

where  $n_A$  is the Avogadro number. Let us compare this probability with the probability of decay. If  $N$  is produced at the distance  $l$  from a detector and the size of a detector is  $d$ , then the probability of decay is:

$$P_{\text{decay}} = e^{-l/\lambda_N} \left( 1 - e^{-d/\lambda_N} \right). \quad (15)$$

For fixed  $l$  and  $d$  maximum is achieved at

$$\lambda_N = d [\text{Log}(1 + d/l)]^{-1} \approx l, \quad (16)$$

where the second equality is for  $d \ll l$ . The probability at  $\lambda = l$  and typical values of  $d$  and  $l$  equals

$$P_{\text{decay}}^{\text{max}} = \frac{d}{el} \sim 10^{-2}. \quad (17)$$

Therefore, the  $N$ -decay can be substituted by upscattering of  $N$  if  $P_N > 10^{-2}$ , which implies, according to (14), that  $G_N > 10^4 G_F$ . The latter is difficult to realize.

Connecting the two production mechanisms and three decay possibilities listed above we arrive at the following 6 scenarios for  $X = N$ . The number of possibilities further multiplies due to various  $\xi$ .

1)  $M_N D_\xi$ , Mixing - Decay scenario: the heavy neutrino  $N$  produced in the  $K$  and  $\pi$ -decay via mixing in  $\nu_\mu$  and decays as  $N \rightarrow N' + \xi$ . Here  $\xi$  is any state in Eq. (5) except  $e$ , and  $N'$  can be simply a standard neutrino  $\nu$ . Only decays inside the detector give the observable signal.

2)  $M_N D_\nu U_e$ , Mixing - Decay into  $\nu_e$  scenario:  $N$  is produced via mixing and decays with emission of  $\nu_e$ :  $N \rightarrow \nu_e + B$ . Then  $\nu_e$  upscatters in the detector, producing electron.

3)  $M_N D_B D_\xi$ , Mixing-double decay scenario:  $N$  produced via mixing decays invisibly into another new particle  $B$ , which in turn decays into (or with emission of)  $\xi$ . This double decay scenario is characterized by  $U_{\mu 4}$ ,  $m_N$ ,  $\tau_N$ ,  $m_B$ ,  $\tau_B$ .

4)  $U_N D_\xi$ , Upscattering - decay scenario:  $N$  is produced in the  $\nu_\mu$  interactions with particles of medium between the source and the detector and in the detector. Then  $N$  decays in the detector, producing  $\xi$  state. If the interaction of  $N$  with the medium can be neglected, the  $N$  flux is accumulated along the way to a detector. The parameters of this scenario are  $m_N$ ,  $\tau_N$  and  $\sigma_N$ .

5)  $U_N D_\nu U_e$ , Upscattering- decay into  $\nu_e$  scenario:  $N$  produced by the  $\nu_\mu$  upscattering decays with emission of  $\nu_e$ , which then scatters in the detector via CCQE producing  $e$  shower. The

parameters here are  $m_N$ ,  $\tau_N$  and  $\sigma_N$ .

6)  $U_N D_B D_\xi$ , Upscattering - double decay scenario:  $N$  produced by  $\nu_\mu$  upscattering undergoes double decay:  $N \rightarrow B \rightarrow \xi$ . Here parameters are  $\sigma_N$ ,  $m_N$ ,  $\tau_N$ ,  $m_B$ ,  $\tau_B$ .

Scenarios 1, 2, 4, 5 contain two vertices with new particles, Scenarios 3 and 6 are of higher (third) order in the new physics interactions.

Two more scenarios can be identified in which  $\xi$ -state is produced by upscattering of  $N$ . They have additional suppression in comparison to  $\xi$  production in decays. The first is  $M_N U_\xi$  mixing -  $N$  upscattering. Here,  $N$  produced by mixing in  $\nu_\mu$  upscatters in a detector with production of electron:  $N + A \rightarrow e + A'$ . This implies the lepton number violation since  $N$  is mixed in  $\nu_\mu$  but produces  $e$  in interactions. The second is  $U_N U_\xi$  which is double upscattering:  $N$  is produced in upscattering of  $\nu_\mu$  and then upscatters with production of  $\xi$  ( $e$ ).

The 6 scenarios described above are not completely independent from the geometrical point of view and even coincide in certain limits of parameters. Thus, for short lifetime of  $B$  we have

$$U_N D_\xi \approx U_N D_B D_\xi, \quad (18)$$

with the only difference that in the double decay case the invariant mass of particles in the final state is fixed by the mass of  $N$ .

For  $X = B$  we have the same mechanisms of production and decay. Kinematically, they coincide with scenarios for  $N$ , but differ from model building side. For bosons, we have the following scenarios: (i)  $M_B D_\xi$  production of  $B$  in a decay pipe in meson decays and further decay  $B \rightarrow \xi$ ,  $B \rightarrow B'\xi$  (ii)  $M_B D_\nu D_e$  when  $B$ - decays with emission of  $\nu_e$ ,  $B \rightarrow \nu_e \bar{\nu}_e$  or  $B \rightarrow \nu_e N'$  (iii)  $M_B D'_B D_\xi$  - double decay which probably is non-minimal and complicated version of (i); Three other mechanisms differ from (i - iii) by  $B$  production mechanism: instead of decays in the pipe,  $B$  is produced via  $\nu_\mu$ - upscattering in a detector and the surrounding medium: (iv)  $U_B D_\xi$  - with  $B$  decays as in (i), see Ref. [12], (v)  $U_B D_\nu D_e$  -  $B$ -decay into  $\nu_e$  which in turn produces  $e$  in CCQE in a detector. (vi)  $U_B D'_B D_\xi$  - double decay which as (iii) is non-minimal version of (iv).

Throughout the paper we focus on scenarios with  $X = N$ .

### C. Bounds on parameters of upscattering scenarios from timing.

Our predictions for number of events in the detector  $i$  are determined by difference of Mini-BooNE and a detector  $i$ -setup. In particular, the difference of geometries plays crucial role. Therefore, bounds from timing are crucial for our consideration. The bounds are different for scenarios with  $N$  production in the decay pipe via mixing and in a detector via upscattering.

In the first case,  $N$  propagates from the production point in a pipe to the detector, *i.e.* the distance equals baseline  $l$ . In such scenario, a delay of the events produced by  $N$  with respect to signal from usual neutrinos equals

$$\Delta t = \frac{l}{c} \left[ \frac{1}{\sqrt{1 - y^2}} - 1 \right] \approx \frac{l}{c} \frac{m_N^2}{2E_N^2}, \quad (19)$$



where  $y \equiv \frac{m_N}{E_N}$  and the last equality is for  $y \ll 1$ . Numerically, we have

$$\Delta t = 8 \text{ ns} \left( \frac{l}{500 \text{ m}} \right) \left( \frac{m_N}{0.1 \text{ GeV}} \right)^2 \left( \frac{1 \text{ GeV}}{E_N} \right)^2. \quad (20)$$

Using  $E_N = 0.3 \text{ GeV}$  and  $\Delta t = 1 \text{ ns}$  we find the upper bound on the mass,  $m_N < 10 \text{ MeV}$ . For scenarios with  $X_s$  production in a decay pipe, the timing gives a strong bound on its mass:  $m_N, m_B < 10 \text{ MeV}$ . In the case of  $N, B$  decays this bound leads to very forward excess of events in MiniBooNE which contradicts data. (The observed angular spectrum of the MiniBooNE excess requires  $m_N$  to be above  $200 \text{ MeV}$  [19], such that the dominant production of heavy neutrinos are kaon decays at the source.) Such a possibility can still be considered if there is two component interpretation of the angular distribution of the excess (which, in fact, is favored by recent data). One component is nearly isotropic due to e.g. underestimated background and new physics contribution peaks in the forward direction. Keeping this in mind we will still consider such scenarios.

Another possibility is that the final state  $\xi$  is produced via upscattering of  $X_s$ . In the upscattering case, the typical decay length is smaller than the detector size  $\lambda_N < d$ . Then, we should use  $l = \lambda_N = c\tau^0 E_N/m_N$  as an conservative estimate for the distance of decay. Using expression (19) for the delay we can write the lifetime of  $N$  as

$$(c\tau^0)_\Delta = c\Delta t y \left[ \frac{1}{\sqrt{1-y^2}} - 1 \right]^{-1}. \quad (21)$$

For  $y \ll 1$  this gives

$$(c\tau^0)_\Delta \approx 2c\Delta t \frac{E_N}{m_N}.$$

To get a delay smaller than a given  $\Delta t$ , the lifetime should be

$$c\tau^0 < (c\tau^0)_\Delta = 2c\Delta t \frac{E_N}{m_N}. \quad (22)$$

Taking  $\Delta t = 1 \text{ ns}$  and  $E_N = 0.8 \text{ GeV}$  we obtain the following upper bounds on  $c\tau^0$  for values of  $m_N$  that we use in computations

$$m_N = (0.15, 0.25, 0.35) \text{ GeV}, \quad c\tau^0 < (3.2, 1.92, 1.37) \text{ m}. \quad (23)$$

#### D. Signature factors and efficiencies

Experiments observe events of various types  $s^i$ , which depend on features of a detector  $i$ . We will call them signatures. In particular, MiniBooNE observes 1 and 2 showers events, while ND T2K with better particle ID can observe  $-\gamma$  showers,  $e-$  showers (tracks),  $2-$  showers events:

$$s^{MB} = \{1sh, 2sh\}, \quad s^{ND} = \{\gamma-sh, e-sh, 2sh\}. \quad (24)$$

Because of misidentification, the observed events do not correspond uniquely to certain original states  $\xi$ . To describe this, we introduce the signature factors  $f_{\xi-s^i}^i$  which give fraction of cases in which a given state  $\xi$  shows up as  $s^i$  event in the  $i$ -detector. Equivalently,  $f_{\xi-s^i}^i$  can be considered as the probability that a state  $\xi$  will show up as  $s^i$  event.



$f_{\xi-s^i}^i$  depends on parameters of  $\xi$  state - energies of particles, masses, as well as on properties of detectors. For MiniBooNE, single electron will be seen as 1sh event, namely  $f_{e-1sh}^{MB} = 1$ . Similarly, for  $\gamma$ :  $f_{\gamma-1sh}^{MB} = 1$ . Also  $e^+e^-$  state can show up as 1 shower event but  $f_{ee-1sh}^{MB} < 1$  and the fraction depends on the kinematical variables of  $e^+$  and  $e^-$ .

The numbers of events depend also on experimental reconstruction efficiency for a given signature  $\epsilon_s^i(E_N, m_N)$ , which is an empirical function. It depends on properties of the signature, such as energies and angles. For simplicity, we take it to be a constant value for a given experiment and signature.

### III. NUMBERS OF NEW PHYSICS EVENTS IN THE GENERIC SCENARIOS

Notice that for fast  $B$  decay, the scenario 3) of Section II B, *i.e.*  $M_N D_B D_\xi$ , is reduced to the first scenario  $M_N D_\xi$ . The scenario 5) has two upscattering vertices and therefore the corresponding number of events has an additional smallness. In what follows we will consider the remaining 4 scenarios with new heavy neutrino.

For each of these, we will derive general expressions for the number of events  $N_{\xi-s^i}^i$  of different types,  $s^i$ , originated from a given state  $\xi$  in a detector  $i$ . If these events are generated in the decays of heavy neutrinos, they are proportional to the number of  $N$  decays:

$$N_{\xi-s^i}^i = N_N^i Br(N \rightarrow \xi) f_{\xi \rightarrow s^i}^i. \quad (25)$$

Here  $Br(N \rightarrow \xi)$  is the branching ratio of the  $N$  decay with  $\xi$  in the final state. We will consider dependence of number of events on the parameters of the scenarios, mainly,  $m_N$  and  $\tau_N^0$ , as well as  $\sigma_N$  (for upscattering cases).

We normalize the numbers of events of type  $\xi - s^i$  in a given detector  $i$  to the MB excess, *i.e.* to  $N_{1sh}^{MB}$ :

$$N_{\xi,exp}^i = N_{1sh,exp}^{MB} \frac{N_{\xi-s^i}^i}{N_{1sh}^{MB}}, \quad (26)$$

where  $N_{exp}^{MB} = 638$  (1) is the sum of the  $\nu$  and  $\bar{\nu}$  excesses of events observed by MB,  $N_{1sh}^i$  and  $N_{1sh}^{MB}$  are the theoretical numbers of events. In this way we ensure that a given scenario explains the MB excess. Furthermore, various factors cancel in the ratio of predictions (such as mixing parameter, coupling constants, normalization of cross sections, *etc.*).

According to (26), the signal in  $i$ -detector predicted in terms of the MiniBooNE excess is determined by difference (ratio) of theoretical values of signals in  $i$ - and MiniBooNE detectors. Recall that we are considering experiments with setups that are qualitatively the same.

Apart from the external parameters such as POT,  $\epsilon$ , detector mass  $M$ , the difference stems from geometry and related parameters: the length of decay pipe  $l_p^i$ , the distance between the end of the tunnel to the detector  $b^i$ , so that  $l^i = l_p^i + b^i$  is the total baseline, the effective length of a detector  $d^i$ , the energy spectra, and masses of particles involved, in particular  $m_N$ ,  $m_B$ . The difference depends on characteristics of detectors and first of all, particle ID which is encoded in the signature factors. Other characteristics cancel.

For simplicity, superscripts  $i$  indicating experiment/detector will be omitted. We will recover them when needed.

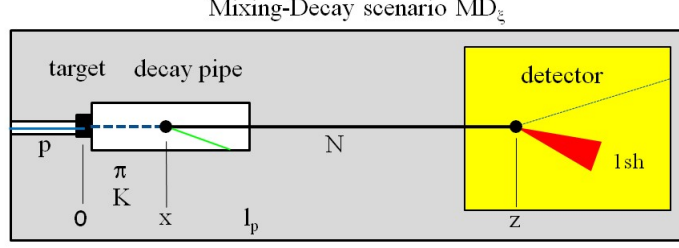


FIG. 1. *Mixing-Decay scenario*. Black blobs show the interaction points, the red triangle denotes the EM shower,  $l_p$  is the length of decay pipe.

### A. Mixing-Decay, $MD_\xi$ — scenario

Recall that in this scenario (schematically shown in Fig. 1), the heavy neutrinos,  $N$ , are produced in  $\pi$  and  $K$  decays via mixing in  $\nu_\mu$  in the decay tunnel. Then  $N$  decay ( $N \rightarrow \xi + \nu$ ) along the baseline, from  $N$ -production point in the tunnel, outside the pipe to a detector. Mainly, decays in a detector produce the observable events. One expects lateral phenomena: some signal from  $N$ -decay outside a detector.

This mechanism gains since no interactions with matter in a detector is needed. But it loses because  $N$  decays everywhere. As we discussed, the optimal decay length, which maximizes signal, is comparable to the baseline  $\lambda \sim l$ .

Probabilities of the three processes involved are factorized since  $N$  is produced in the decay pipe,  $x = 0 \div l_p$ , and the observed events are due to  $N$ -decays only in a detector  $l \div (l + d)$ . Let us consider them in order.

1. Formation of the  $N$ -flux in the pipe: Recall that due to arrival time restrictions,  $m_N < 10$  MeV, the neutrino  $N$  is mainly produced in  $\pi$  decays via mixing. One should take into account the  $N$  decay before the end of pipe. Integration over the coordinate along the decay tunnel gives the  $N$ -flux at the exit from the pipe ( $x = l_p$ ). For  $\pi$  of energy  $E_\pi$  and  $N$  of energy  $E_N$  we have

$$\frac{d\phi_N(l_p)}{dE_N dE_\pi} = |U_{\mu 4}|^2 \frac{d\phi_\pi^0(E_\pi)}{dE_\pi} \frac{d\Gamma(E_\pi, E_N)}{\Gamma_\pi^{tot} dE_N} \left(1 - \frac{\lambda_\pi}{\lambda_N}\right)^{-1} \left[e^{-l_p/\lambda_N} - e^{-l_p/\lambda_\pi}\right], \quad (27)$$

where  $d\phi_\pi^0(E_\pi)/dE_\pi$  is the flux of  $\pi$  mesons at the target,  $\Gamma_\pi^{tot} = 1/\lambda_\pi$  is the total decay rate of  $\pi$ ,

$$\lambda_N(E_N, m_N) = (p_N/m_N) c\tau_N^0, \quad \lambda_\pi(E_\pi, m_\pi) = (p_\pi/m_\pi) c\tau_\pi^0, \quad (28)$$

are the decay lengths of  $N$  and  $\pi$ -meson, respectively,  $\tau_\pi^0, \tau_N^0$  are their lifetimes in the restframes.

Notice that in the limit  $\lambda_N \rightarrow \infty$  (negligible  $N$ -decay) the last two factors in (27) are reduced to

$$\left(1 - e^{-l_p/\lambda_\pi}\right), \quad (29)$$

which is nothing but the probability of  $\pi$ -decay in the pipe.

2.  $N$ -flux at the entrance to the detector differs from (27) by survival of  $N$  along distance  $b$ :

$$d\phi_N(l_p + b) = d\phi_N(l) = d\phi_N(l_p) e^{-b/\lambda_N}. \quad (30)$$

3. Number of  $N$  decays in a detector, which gives the number of observed events, equals

$$dN = f(E_N) \epsilon A d\phi_N(l) (1 - e^{-d/\lambda_N}). \quad (31)$$

Plugging in (31) explicit expressions of the factors from (30) and (27) and integrating over the energies  $E_K$  and  $E_N$  we obtain

$$N_{\xi-s} = \epsilon A |U_{\mu 4}|^2 \int dE_N f_{\xi-s}(E_N) \int dE_\pi \frac{\phi_\pi^0(E_\pi)}{dE_\pi} \frac{d\Gamma(E_\pi, E_N)}{\Gamma_\pi^{tot} dE_N} P_{dec}(E_\pi, E_N), \quad (32)$$

where

$$P_{dec}(E_\pi, E_N) = e^{-b/\lambda_N} \left(1 - e^{-d/\lambda_N}\right) \left(1 - \frac{\lambda_\pi}{\lambda_N}\right)^{-1} \left[e^{-l_p/\lambda_N} - e^{-l_p/\lambda_\pi}\right], \quad (33)$$

is the decay factor.

Since  $\lambda_\pi \ll \lambda_N$  and  $\lambda_\pi < l_p$ , the dependence of  $P_{dec}$  on  $E_\pi$  is weak and  $P_{dec}$  can be moved out of integration over  $E_\pi$ , taken as a function of some effective  $\bar{E}_\pi$ . Then, by introducing the  $N$  flux at the target

$$\frac{\phi_N^0(E_N)}{dE_N} = |U_{\mu 4}|^2 \int dE_\pi \frac{d\phi_\pi^0(E_\pi)}{dE_\pi} \frac{d\Gamma(E_\pi, E_N)}{\Gamma_\pi^{tot} dE_N}, \quad (34)$$

Eq. (32) can be reduced to

$$N_{\xi-s} = \epsilon A |U_{\mu 4}|^2 \int dE_N \frac{d\phi_N^0(E_N)}{dE_N} f_{\xi-s}(E_N) P_{dec}(\bar{\lambda}_\pi). \quad (35)$$

Here  $\bar{\lambda}_\pi = c\tau_\pi^0 \bar{E}_\pi / m_\pi$ .

If  $d \ll \lambda_N$ , the probability of decay in a detector is much smaller than 1 and the decay factor becomes

$$P_{dec} \approx \frac{d}{\lambda_N} e^{-l/\lambda_N}. \quad (36)$$

Qualitatively, the dependence of numbers of events given in (26) can be understood by considering the ratio of the decay factors (36) for a given experiment  $i$  and MiniBooNE taken at certain effective energies in experiments,  $E^i$  and  $E^{MB}$ :

$$r_d \equiv \frac{P_{dec}^i}{P_{dec}^{MB}} = \left(\frac{d^i}{d^{MB}}\right) \left(\frac{E_N^{MB}}{E_N^i}\right) e^{(L^{MB}-L^i)/c\tau^0}, \quad (37)$$

where

$$L^i \equiv l^i \frac{m_N}{E_N^i}. \quad (38)$$

According to (38), the dependence of  $N_s^i$  on  $c\tau^0$  is determined by baseline lengths and not sizes of detectors. Among detectors we consider,  $l$  is the longest and  $E_N$  is the smallest in MiniBooNE, therefore  $L^{MB} > L^i$ . Numerically,

$$L^{MB} = 6.7 \text{ m} \left(\frac{m_N}{10\text{MeV}}\right). \quad (39)$$

For  $c\tau^0 \gg (L^{MB} - L^i)$ , the ratio  $r_d$ , and consequently  $N_{\xi-s}^i$ , does not depend on  $c\tau^0$ . In this limit  $N$ -decays before the detector can be neglected. Here  $r_d$  also does not depend on  $m_N$ . With

decrease of  $c\tau^0$ , first the MiniBooNE detection is affected by the  $N$ -decays and then  $i$  detector does. As a result, at

$$c\tau^0 < c\tau_{up}^0 \equiv L^{MB} - L^i = m_N \left( \frac{l^{MB}}{E_N^{MB}} - \frac{l^i}{E_N^i} \right), \quad (40)$$

the ratio turns up and shows the exponential grow (in agreement with figures in Section V). With the increase of  $m_N$ , the upturn shifts to larger energies. The dependence of the number of events on  $m_N$  is determined in addition by the  $m_N$ -dependence of the  $N$  fluxes, cross sections and signature factors.

In asymptotics,  $c\tau^0 \gg \Delta L$ , which corresponds to very big decay length of  $N$ , the theoretical number of events can be estimated using (35) and (36) as follows:

$$N_{\xi-s} = \epsilon A d \frac{m_N}{c\tau^0} |U_{\mu 4}|^2 \int dE_N \frac{1}{E_N} f_{\xi-s}(E_N) \frac{d\phi_N^0(E_N)}{dE_N}. \quad (41)$$

Then, assuming that  $f_{\xi-s}(E_N) = \text{const}$ , the expected number of events (26) can be written as

$$N_{\xi-s}^i = N_{exp}^{MB} \left( \frac{V^i}{V^{MB}} \right) \left( \frac{E_N^{MB}}{E_N^i} \right) \left( \frac{f_{\xi-s}^i}{f_{1sh}^{MB}} \right) \left( \frac{\epsilon_{\xi-s}^i}{\epsilon_{1sh}^{MB}} \right) \left( \frac{\phi_N^i}{\phi_N^{MB}} \right), \quad (42)$$

where  $V^i = A^i d^i$  is the volume of a detector  $i$  and  $\phi_N^i \propto \phi_\nu^i$  is the integral flux of  $N$  in detector  $i$ .

### B. Upscattering - decay, $U_N D_\xi$ - scenario

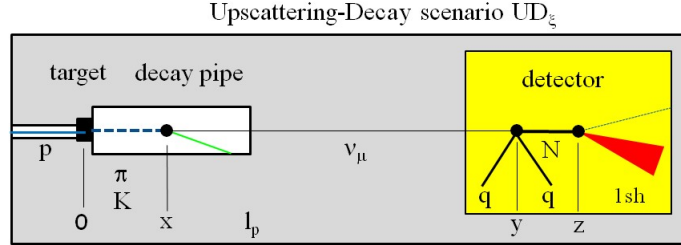


FIG. 2. *Upscattering-Decay scenario*. Black blobs show the interaction points, red triangle denotes the EM shower,  $l_p$  is the length of decay pipe.

In this scenario (schematically shown in Fig. 2)  $N$  is produced by  $\nu_\mu$  upscattering on material along a baseline and then decays  $N \rightarrow \nu + \xi$ . The  $N$ -decays inside a detector give the observable signal, while  $N$  itself can be produced both in the detector and in the surrounding material. If the decay length of  $N$  is  $\lambda_N \gg d$ , a large part of the  $N$  flux can be formed outside a detector.

Let us first consider production and sequential decay of  $N$  inside a detector. Integrating over the detector length and over energies of  $\nu_\mu$  and  $N$  we obtain the number of  $s$ -events

$$N_{\xi-s}^{in} = \epsilon V_d n_d \int dE_N f_{\xi-s}(E_N) \frac{d\phi_N^\sigma(E_N)}{dE_N} \left[ 1 - \frac{\lambda_N}{d} (1 - e^{-d/\lambda_N}) \right], \quad (43)$$

where  $V_d \equiv A d$  and

$$\frac{d\phi_N^\sigma(E_N)}{dE_N} \equiv \int dE_\nu \frac{d\phi_\nu(E_\nu)}{dE_\nu} \frac{d\sigma(E_\nu, E_N)}{dE_N}. \quad (44)$$

Notice that  $nd\phi_N^\sigma(E_N)/dE_N$  is the density of  $N$ -flux produced in detector. In the prefactor of (43) the product  $Adn = V_d n = M_d$  gives the mass of a detector.

The expression in the brackets of (44) can be interpreted as the decay factor (the probability of decay):

$$P_{dec}^{in} = 1 - \frac{\lambda_N}{d} \left(1 - e^{-d/\lambda_N}\right). \quad (45)$$

In the asymptotics,  $\lambda_N \gg d$ , this factor converges to

$$P_{dec}^{in} \approx \frac{d}{2\lambda_N}, \quad (46)$$

and in the opposite case,  $\lambda_N \ll d$ , we have  $P_{dec} \rightarrow 1$ .

Let us find the contribution to the number of events in a detector from  $N$  produced in surrounding material (dirt). We denote by  $\Delta$  the distance between a detector and dirt (usually the air in a detector pit). For simplicity we consider uniform surrounding medium with density  $n_b$ . The  $N$ -flux produced by  $\nu_\mu$  in the dirt of length  $b$ , that enters later in a detector equals

$$\frac{d\phi_N}{dE_N} = n_b A \frac{d\phi_N^\sigma(E_N)}{dE_N} \lambda_N e^{-\Delta/\lambda_N} \left(1 - e^{-b/\lambda_N}\right). \quad (47)$$

Here we made integration over the distance from 0 (the end of pipe) to  $b$  taking into account decay of  $N$ .  $\phi_N^\sigma(E_N)$  is defined in (44). The factors in (47), that depend on  $\lambda_N$ , reduce to  $b$  for stable  $N$ :  $\lambda_N \rightarrow \infty$  and to  $\lambda_N$  for  $\lambda_N \rightarrow 0$ . The number of  $N$ -decays inside a detector, which gives the number of observable events, equals

$$N_{\xi-s}^{out} = \epsilon N_b \int dE_N \frac{d\phi_N^\sigma(E_N)}{dE_N} f_{\xi-s} P_{dec}^{out}(E_N), \quad (48)$$

where  $N_b = n_b A b$  is the number of scatterers in medium and

$$P_{dec}^{out}(E_N) = \frac{\lambda_N}{b} e^{-\Delta/\lambda_N} \left(1 - e^{-b/\lambda_N}\right) \left(1 - e^{-d/\lambda_N}\right), \quad (49)$$

is the decay factor. Here  $e^{-\Delta/\lambda_N}$  is the survival probability of  $N$  between the end of dirt and the detector. In general, if a detector and a pit have non-rectangular form, the parameters  $\Delta$  and  $d$  depend on distance from center of the setup  $h$  and one needs to make integration over  $h$ .

In the limit  $b \gg \lambda_N$  we obtain

$$N_{\xi-s}^{out} = A n_b \epsilon \int dE_N \lambda_N \frac{d\phi_N^\sigma(E_N)}{dE_N} f_{\xi-s} e^{-\Delta/\lambda_N} \left(1 - e^{-d/\lambda_N}\right). \quad (50)$$

In this limit, the  $N$  flux is collected along the distance  $\lambda_N$  in front of detector.

The total number of events due to  $N$  produced in a detector and surrounding materials can be written as

$$N_{\xi-s}^{tot} = A d n_d \epsilon \int dE_N \frac{d\phi_N^\sigma(E_N)}{dE_N} f_{\xi-s} \left( P_{dec}^{in} + \frac{b n_b}{d n_d} P_{dec}^{out} \right), \quad (51)$$

or explicitly,

$$N_{\xi-s}^{tot} = A d n_d \epsilon \int dE_N \frac{d\phi_N^\sigma(E_N)}{dE_N} f_{\xi-s} \left\{ 1 + \frac{\lambda_N}{d} \left(1 - e^{-d/\lambda_N}\right) \left[ \frac{n_b}{n_d} e^{-\Delta/\lambda_N} \left(1 - e^{-b/\lambda_N}\right) - 1 \right] \right\}. \quad (52)$$

In the limit  $b \gg \lambda_N$  the number of events equals

$$N_{\xi-s}^{tot} = Adn_d \epsilon \int dE_N \frac{d\phi_N^\sigma(E_N)}{dE_N} f_{\xi-s} \left[ 1 + \frac{\lambda_N}{d} \left( 1 - e^{-d/\lambda_N} \right) \left( e^{-\Delta/\lambda_N} \frac{n_b}{n_d} - 1 \right) \right]. \quad (53)$$

For  $\lambda_N > d$  and  $\Delta < \lambda_N$  the contribution from dirt can be much (several times) larger than the one from a detector.

Let us consider the dependence of numbers of events (26) on  $c\tau^0$  which is largely determined by the ratios of decay factors for the detector  $i$  and MiniBooNE taken at certain effective energies  $E_N^{MB}$  and  $E_N^i$ . For the contribution due to  $N$  production inside a detector  $i$ , the dependence of the number of events on  $c\tau^0$  is determined by the ratio of decay factors  $P_{dec}^{in}$  (45) which can be written as

$$r_{dec} = \frac{1 - \frac{c\tau^0}{D^i} \left( 1 - e^{-D^i/c\tau^0} \right)}{1 - \frac{c\tau^0}{D^{MB}} \left( 1 - e^{-D^{MB}/c\tau^0} \right)}, \quad (54)$$

where

$$D^i \equiv d^i \frac{m_N}{E^i}, \quad (55)$$

are the reduced sizes of detectors ( $d/\lambda = D/c\tau^0$ ). Among experiments we consider, MiniBooNE has the largest reduced size  $D^{MB} > D^i$ . Numerically, for MiniBooNE ( $d_{MB} = 8$  m and  $E_N^{MB} = 0.8$  GeV)

$$D_{MB} = 1.5 \text{m} \left( \frac{m_N}{0.15 \text{GeV}} \right). \quad (56)$$

Taking this into account we find

(i) for  $c\tau^0 < D^i$  m both decay probabilities (for MiniBooNE and  $i$ ) are close to 1, so that  $r_{dec} \approx 1$ . Consequently, the ratio of number of events does not depend on  $c\tau^0$ . It also does not depend on  $m_N$ . The dependence on  $m_N$  follows from fluxes and cross-sections.

(ii) In the interval  $D^i < c\tau^0 < D^{MB}$ ,  $N$  still has space to decay in MiniBooNE and  $P_{dec}^{MB} \sim 1$ , while the  $N$  decay length becomes larger than  $i$  detector length and therefore  $P^i$  decreases. As a result, the number of  $i$  detector events should decrease.

(iii) For  $c\tau^0 > D_{MB}$ , in both detectors there is only partial decay and the ratio of decay factors converges to

$$r_{dec}^\infty = \frac{P_{dec}^i}{P_{dec}^{MB}} = \frac{D^i}{D^{MB}} = \frac{d^i E_N^{MB}}{d^{MB} E_N^i}. \quad (57)$$

Again, dependence on  $c\tau^0$  as well as on  $m_N$  disappears.

In the limit  $c\tau^0 \rightarrow 0$  the decay factors  $P_{dec} \approx 1$  and the number of events can be estimated as

$$N_{\xi-s}^{ND} = N_{1sh,exp}^{MB} \left( \frac{M^i}{M^{MB}} \right) \left( \frac{f_{\xi-s}^{ND}}{f_{1e}^{MB}} \right) \left( \frac{\epsilon_{\xi-s}^i}{\epsilon_{1sh}^{MB}} \right) \left( \frac{\sigma^i}{\sigma^{MB}} \right) \left( \frac{\phi_\nu^i}{\phi_\nu^{MB}} \right). \quad (58)$$

as  $\phi_\nu^i \propto (POT)^i$  [20].

For  $N$  production in the dirt and decaying in a detector we have

$$r_{dec} = \frac{\frac{\lambda_N^i}{d^i} \left( 1 - e^{-d^i/\lambda_N^i} \right) \frac{n_b^i}{n_d^i} e^{-\Delta^i/\lambda_N^i} \left( 1 - e^{-b^i/\lambda_N^i} \right)}{1 + \frac{\lambda_N^{MB}}{d^{MB}} \left( 1 - e^{-d^{MB}/\lambda_N^{MB}} \right) \left[ \frac{n_b^{MB}}{n_d^{MB}} e^{-\Delta/\lambda_N} \left( 1 - e^{-b^{MB}/\lambda_N^{MB}} \right) - 1 \right]}. \quad (59)$$

Now, the decay factor (49) is proportional to  $\lambda_N$ , in the limit  $c\tau^0 \rightarrow 0$  the ratio equals

$$r_{dec}^0 = \frac{\lambda_N^i}{d^i} \frac{n_b^i}{n_d^i}, \quad (60)$$

and contribution from outside vanishes.

In the limit  $c\tau^0 \rightarrow \infty$

$$r_{dec}^\infty = \frac{n_d^{MB}}{n_d^i} \frac{n_b^i}{n_b^{MB}} \frac{b^i}{b^{MB}} \frac{\lambda_N^{MB}}{\lambda_N^i}.$$

That is, the contribution converges to constant.

### C. Upscattering - Double Decay scenario, $UD_B D_\xi$ -scenario.

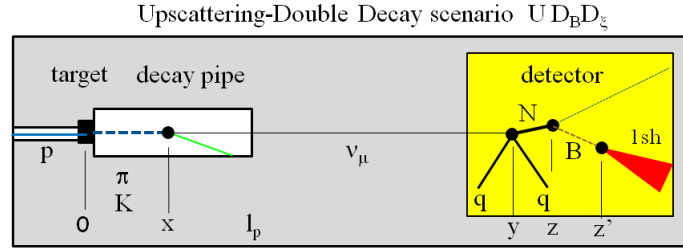


FIG. 3. *Upscattering Double Decay scenario*. Black blobs show the interaction points, red triangle is the EM shower,  $l_p$  is the length of decay pipe.

This scenario (schematically shown in Fig. 3) is very similar to the previous one described in Section III B when  $B$  decays promptly. In such case, the only but rather relevant difference is in the mass of a particle decaying into  $\xi$ . In this scenario, this is the mass of a gauge boson,  $B$ , which can be substantially smaller than the mass of  $N$ . While in Section V we will show results for short  $B$  lifetime, the investigation of long lived  $B$  in relation to MiniBooNE excess is left for the future work.

### D. Mixing - Decay into $\nu_e$ , $MD_\nu$ -scenario.

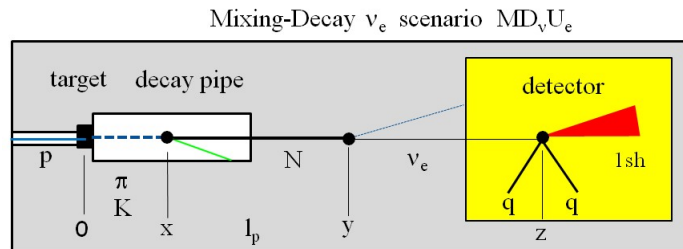


FIG. 4. *Mixing decay into  $\nu_e$  scenario*. Black blobs show the interaction points, red triangle is the EM shower,  $l_p$  is the length of decay pipe.



This scenario (schematically shown in Fig. 11) essentially provides additional source of  $\nu_e$  at low energies. Therefore, there is no restrictions from angular dependence of the observed MiniBooNE events and  $N$  can be light enough to be produced in the  $\pi$ -decay. Since flux of pions is 2 orders of magnitude larger than flux of  $K$ -mesons, the scenario will allow to obtain required number of events at lower new physics couplings. Relatively light  $N$  is produced via mixing with  $\nu_\mu$  in  $\pi$ -decays and then decays into  $\nu_e$  and a new light scalar or vector boson along the beamline  $N \rightarrow \nu_e + B$ . In turn, these bosons  $B$  may decay into  $\nu_e \bar{\nu}_e$  pair, thus enhancing the  $\nu_e$  flux at low energies. Here we have more interaction points in contrast to previous scenarios (although in one point interactions are standard).

Since  $N$  can decay already in the decay tunnel, the consideration should start from  $\pi$ -decay as in the  $M_N D_\xi$  scenario of section Section III A. In contrast to  $MD_\xi$ ,  $N$  decays in the pipe do contribute to the signal in a detector, since  $\nu_e$  are stable and can travel to a detector. This requires different consideration from  $MD_\xi$ .

Let  $\phi_\pi^0$  be the pion flux produced in a proton target. Then, the flux of pions at a distance  $x$  from the target equals

$$\frac{d\phi_\pi(x)}{dE_\pi} = \frac{d\phi_\pi^0(x)}{dE_\pi} e^{-x/\lambda_\pi}. \quad (61)$$

Here  $\lambda_\pi(E_\pi) = c\tau_\pi^0 E_\pi/m_\pi$  is the decay length of pion. The  $N$ -flux at a distance  $y$  from the target ( $y > x$ ) is

$$\frac{d\phi_N(y)}{dE_N} = |U_{\mu N}|^2 \int dE_\pi \frac{d\phi_\pi^0(x)}{dE_\pi} \frac{d\Gamma(E_\pi, E_N)}{\Gamma_\pi^{tot} dE_N} \int_0^X \frac{dx}{\lambda_\pi} e^{-x/\lambda_\pi} e^{-(y-x)/\lambda_N}, \quad (62)$$

where  $X = y$  for  $y \leq l_p$ , and  $X \geq l_p$ , for  $x \leq l_p$ , reflecting the fact that pions do not decay beyond the decay pipe. Two regions of integration correspond to  $N$ -decays inside and outside the tunnel. In eq. (62) the branching ratio of the decay equals  $B_N = |U_{\mu N}|^2$  with  $U_{\mu N}$  being the mixing matrix element (since  $N$  is light in this scenarios, kinematic factors can be neglected). The second exponent under integral is the probability that  $N$  does not decay between production point  $x$  and a given point  $y$ .

Introducing

$$\frac{d^2\phi'_N}{dE_N dE_\pi} \equiv \frac{d\phi_\pi^0}{dE_\pi} \frac{d\Gamma(E_\pi, E_N)}{\Gamma_\pi^{tot}(E_\pi) dE_N}, \quad (63)$$

we can rewrite (62) as

$$\frac{d\phi_N(y)}{dE_N} = |U_{\mu N}|^2 \int dE_\pi \frac{d^2\phi'_N(y)}{dE_N dE_\pi} \int_0^X \frac{dx}{\lambda_\pi} e^{-x/\lambda_\pi} e^{-(y-x)/\lambda_N}. \quad (64)$$

The  $\nu_e$  flux from  $N$  decay in the point  $z$  of a detector ( $z$  is the distance from the front edge of a detector) equals

$$\frac{\phi_\nu(z)}{dE_\nu} = \int_0^{l_t+b+z} \frac{dy}{\lambda_N} \frac{d\phi_N(y)}{dE_N} \frac{d\Gamma_N(y)}{\Gamma_N^{tot} dE_\nu}. \quad (65)$$

Finally, the number of  $e$ -showers in a detector equals

$$N_{e-1sh} = A n_d \epsilon \int dE_\nu \sigma(E_\nu) \int_0^d dz \frac{\phi_\nu(z)}{dE_\nu}. \quad (66)$$

Here, the signature factor is  $f \approx 1$  since  $\xi = e$ , and misidentification can be neglected. Also, we did not introduce integration over the electron momentum, considering that all electrons, that appear, produce the observable signal. (Otherwise one should use the differential neutrino cross-section  $d\sigma(E_\nu, E_e)/dE_e$  and perform integration over  $E_e$  from certain experimental threshold energy, say  $E_e = 100$  MeV).

Plugging (62) into Eq. (65), and then (65) into (66) and performing integrations over spatial coordinates we obtain:

$$N_{e-1sh} = \epsilon A d n_d |U_{\mu N}|^2 \int dE_\nu \sigma^{CC}(E_\nu) \int dE_N f_{e-1sh}(E_N) \frac{d\Gamma_N(E_N, E_\nu)}{\Gamma_N^{tot} dE_\nu} \int dE_\pi \frac{d\phi_\pi^0(E_\pi)}{dE_\pi} \frac{d\Gamma_\pi(E_\pi, E_N)}{\Gamma_\pi^{tot} dE_N} P_{dec}(\lambda_\pi, \lambda_N), \quad (67)$$

where the decay factor equals

$$P_{dec} = \left[ 1 - e^{-l_p/\lambda_\pi} - g(\lambda_\pi, \lambda_N) \frac{\lambda_N}{d} e^{-b/\lambda_N} \left( 1 - e^{-d/\lambda_N} \right) \right]. \quad (68)$$

Here

$$g(\lambda_\pi, \lambda_N) = \left( 1 - \frac{\lambda_\pi}{\lambda_N} \right)^{-1} \left[ e^{-l_p/\lambda_N} - e^{-l_p/\lambda_\pi} \right]. \quad (69)$$

If  $d \ll \lambda_N$ , the equation (68) reduces to

$$P_{dec} \approx \left( 1 - e^{-l_p/\lambda_\pi} - g e^{-b/\lambda_N} \right). \quad (70)$$

Consider two limits of this result:

1)  $\lambda_N \rightarrow 0$  (very fast  $N$ -decay) we have

$$P_{dec} \approx \left( 1 - e^{-l_p/\lambda_\pi} \right), \quad (71)$$

which is nothing but a decay probability of pions in the tunnel. It gives the  $\nu_\mu$  flux at a detector.

2)  $\lambda_N \rightarrow \infty$  (very slow  $N$ -decay): in the lowest order in  $l/\lambda_N$  we find

$$P_{dec} \approx \left( 1 - e^{-l_p/\lambda_\pi} \right) \frac{l^{eff}}{\lambda_N}, \quad (72)$$

where  $l^{eff}$  is the effective baseline:

$$l^{eff} \equiv b + l_p \left( 1 - e^{-l_p/\lambda_\pi} \right)^{-1} - \lambda_\pi. \quad (73)$$

For  $\lambda_\pi \rightarrow 0$  we have  $l^{eff} = b + l_t$ , whereas for  $\lambda_\pi \rightarrow \infty$ ,  $l^{eff} = b$ . For a typical situation  $\lambda_\pi = l_t$  we find

$$l^{eff} = b + l_t (e - 1)^{-1} \approx b + 0.58 l_t. \quad (74)$$

For  $c\tau^0 \rightarrow 0$ , the ratio of decay factors  $r_{dec} \rightarrow 1$  while for  $c\tau^0 \rightarrow \infty$

$$r_{dec}^\infty = \frac{E^i}{E^{MB}} \frac{z^i (b^i + \lambda_\pi^i) + l_p^i}{z^{MB} (b^{MB} + \lambda_\pi^{MB}) + l_p^{MB}}, \quad (75)$$

where  $z^i = (1 - e^{l_p^i/\lambda_\pi^i})$ . Consequently, in both limits the number of events does not depend on  $c\tau^0$ .

#### IV. SIGNATURE FACTORS, CROSS-SECTIONS, EXPERIMENTS AND BOUNDS.

The key idea is that new physics scenarios that explain the MiniBooNE excess should produce visible numbers of events in the near detectors of various neutrino experiments. That will allow us to put bounds on the scenarios. Here we describe the relevant features of the different experiments, theoretical and experimental results. We compute the allowed upper limits on event counts due to new physics.

##### A. Signal

The observable signal is given by a deposit of electromagnetic energy from a final state  $\xi$ . Depending on the particle ID capabilities of a detector  $i$ , a given state  $\xi$  can be (mis-)identified with a number of other particle states. Associated with this identification are detector and analysis efficiencies. Below we describe our approach for quantifying this. We also discuss the cross section input used for the upscattering scenarios.

##### 1. Efficiency

The experiments  $i$  quote signature efficiencies for the signatures  $s^i$  which are, in general, a product of a detector efficiency  $\epsilon_\xi^i$ , a particle (mis-)identification efficiency  $f_{\xi-s^i}^i$  and signal selection efficiency  $\epsilon_{s^i}^i$ .

The detector efficiency  $\epsilon_\xi^i$  quantifies the probability that a final state  $\xi$  is registered in one way or another. In what follows we assume that  $\epsilon_\xi^i = 1$ . The misidentification efficiency or the signature factor  $f_{\xi-s^i}^i$  is the fraction of cases when final state  $\xi$  produces a signature  $s^i$ . The signal selection efficiency  $\epsilon_{s^i}^i$  quantifies the so-called quality cuts (which include kinematic cuts) of the events that are needed to enhance the signal-over-background ratio. These efficiencies depend strongly on the considered signatures and we take their values from experiments.

##### 2. Signature factor

In general, the signature factor includes an integration over the phase space of kinematical variables, and (mis-) identification factors  $I_e^i$ , which depend on the type of detector.

Some detectors can distinguish events induced by a single photon, an  $e^+e^-$  pair, from those induced by a single electron. This is usually accomplished via measuring the energy loss,  $dE/dx$ , over the whole trajectory, or only in its initial part (like in MINER $\nu$ A). Detectors that have a magnetic field, like NOMAD or T2K ND280 also use the bending of tracks for particle ID.

For electrons that are produced by the CCQE  $\nu_e$  scattering on nucleons ( $\xi = e$ ) we can write

$$f_{e-s^i} = \int_{E_e^{th}} dE_e I_{s^i}(E_e) \int dE_\nu \frac{d\sigma(E_\nu, E_e)}{\sigma^{tot} dE_e}, \quad (76)$$

where  $I_{s^i}(E_e)$  is the probability that the electron with energy  $E_e$  will show up as the  $s^i$  event. In experiments capable to disentangle showers induced by  $\gamma$  and  $e$ , the factor  $I_{e-1sh}(E_e) \sim 1$  and due to some misidentification  $I_{\gamma-1sh}(E_e) \neq 0$ .

In experiments that can not distinguish  $e-$  and  $\gamma-$  events, like MiniBooNE, where events are classified as  $1sh$  and  $2sh$ , we have  $I_{1sh}(E_e) = 1$ .

Let us consider final states that originate from  $N$ -decay with energy  $E_N$  and mass  $m_N$ . In general, the signature factor for single shower event can be written as

$$f_{\xi-1sh}^i(E_N, m_N) = \frac{1}{\Gamma_N(E_N, m_N)} \int^{\Pi_f^i} d\Pi_f \frac{d\Gamma_N(E_N, m_N, \Pi_f)}{d\Pi_f}, \quad (77)$$

with the final state phase space  $\Pi_f^i$  in which the produced state  $\xi$  shows up as a single shower event in the experiment  $i$ . Notice that the phase space criteria alone may not be enough and a mis-identification factor should be introduced in addition. Indeed,  $\gamma$  with any given energy can be confused with electron. In general, also angular variables and not only energy should be considered.

For the final state being  $\nu\gamma$  ( $\xi = \gamma$ ), the relevant phase space is above the energy threshold which is for instance  $E_\gamma > 100$  MeV in MiniBooNE (used to suppress cosmic ray backgrounds). In experiments without  $\gamma - e$  identification, and for high energy  $N$ :  $\Pi_f^i$  is nearly entire phase space. Thus  $f_{\gamma-1sh}^i(E_N, m_N) \approx 1$ .

The  $e^+e^-$  pair ( $\xi = e^+e^-$ ) can produce two shower ( $2e$ -showers) events as well as single shower events, if one of the components is missing or if two components are nearly collinear. For several detectors, the unique relevant criterion for differentiation between single and double shower events is the invariant mass of pair,  $W_{ee}$ . If  $W_{ee} < W_c$ , where  $W_c(E_N)$  is a certain critical value, the pair will show up as a single shower event, while for  $W_{ee} > W_c$  – as the two shower event. Here we neglect  $\gamma - e$  misidentification.

When the  $e^+e^-$  pair is created from (3-body) heavy neutrino decays  $N \rightarrow \nu e^+e^-$ ,  $W_{ee}$  is not fixed. The fraction of decays with  $W_{ee} < W_c$ , which appear as single shower event equals:

$$f_{1sh}^i(x, m_N) = \frac{1}{\Gamma(N \rightarrow \nu e^+e^-)} \int_0^{W_c} dW_{ee} \frac{d\Gamma(N \rightarrow \nu e^+e^-)}{dW_{ee}} = \frac{W_c^8 + 2W_c^2 m_N^6 - 2W_c^6 m_N^2}{m_N^8}. \quad (78)$$

We take  $W_c = 30$  MeV for MiniBooNE [21],  $W_c = 5$  MeV for the T2K near detector ND280 (cf. ref. [22]), and we estimate  $W_c = 30$  MeV for PS191. For the other detectors we do not use an invariant mass threshold for our analysis, *i.e.* we assume that  $e^+e^-$  pairs and photons give the same signature. Notice that  $f$  defined in this way does not depend on  $E_N$ , which simplifies computations.

If the  $e^+e^-$  pair appears from 2 body decay of a new boson,  $B \rightarrow e^+e^-$ , the invariant mass  $W_{ee}$  is fixed:  $W_{ee} = m_B$ . Therefore, the signature factor is determined uniquely by the mass of  $B$ . Thus, for  $m_B < W_c$  we have  $f_{ee-1sh}^i = 1$ , while for  $m_B > W_c$ :  $f_{ee-1sh}^i = 0$ . This is realised in scenarios with the decay chain  $N \rightarrow \nu(B \rightarrow e^+e^-)$ , where an on-shell dark photon  $B$  is produced.

For 2 shower signatures we have relation  $f_{ee-2sh}^i = 1 - f_{ee-1sh}^i$ .

## B. Cross-sections and fluxes

In the presence of new physics, the cross sections of heavy or light neutrino interactions generally are model dependent, both in magnitude and in differential shape. Since we compute the ratios of numbers of events, the model dependence of the cross sections mostly cancels. Further, being focused on no specific model, we consider both cases where the interaction is dominantly partially coherent and when it is incoherent. In our calculations, for the partially coherent cross section, we take the mass of the mediator in the upscattering process to be 30 MeV in accord with the benchmark point of [9]. For incoherent case, we calculate the cross section for the mediator mass of 1.25 GeV (using the cookbook presented in [23]) that is the value corresponding to the benchmark point in [7].

For the quasi-elastic scattering of  $\nu_e$  we use the  $\nu_\mu$  upscattering cross section from ref. [24] as a proxy. We expect that the differences due to the different lepton masses should be minor because they are both small compared to the neutrino energies.

### C. Experiments and bounds

#### 1. MiniBooNE

Some information on MB has already been presented in Section II. The total number of muon neutrinos that passed through the MiniBooNE detector in positive (negative) horn polarity mode is  $8.12 \times 10^{17}$  ( $3.1 \times 10^{17}$ ) [25]. This corresponds to the muon neutrino flux per POT:

$$\phi^{MB} = 5.19 \cdot 10^{-10} \text{cm}^{-2} (\text{POT})^{-1}. \quad (79)$$

The relevant parameters of the experimental setup are: the decay pipe length  $l_p^{MB} = 50$  m, baseline  $l^{MB} = 540$  m, average detector length  $d^{MB} = 8$  m and the target mass  $m^{MB} = 800$  t. The average electron reconstruction and selection efficiency is  $\epsilon_{1sh}^{MB} \simeq 10\%$ .

We wish to stress that MiniBooNE is also observing 2 shower events and this can in principle be a powerful probe for scenarios  $\xi = ee$  and  $\xi = \gamma\gamma$ . We have, however, estimated that this search does not yield exclusions as strong as for instance respective search in ND280; the latter will be employed in Section V.

#### 2. T2K ND280

The T2K ND280 (we will call it ND280 for brevity) is sourced by 30 GeV protons that interact with a graphite target [26]. The lengths involved are  $l_p \simeq 100$  m,  $b = 230$  m (dirt), and baseline  $l^{ND} = 280$  meters [27].

ND280, placed at  $2.5^\circ$  off axis, is a multicomponent detector which consists of the following main sub-detectors: the  $\pi^0$  detector P0D, the tracking detector containing the three Time Projection Chambers (TPC) filled in by Ar gas, and two Fine Grained Detectors (FGD) filled in by scintillations. The P0D has a target mass  $m_{P0D}^{ND} = 15.8$  t (when filled with water) and a length  $d_{P0D}^{ND} = 2$  m [28]. Each TPC module has a mass of 0.3 t and a length of 0.9 m. The mass and the length of each FGD are 1.1 t and 0.365 m, correspondingly [29]. Also important is the distance between downstream edge of P0D and the upstream edge of FGD1, which we take to be 1 m. The detector is magnetized with a field strength of 0.2 T, which, together with energy loss tracking, allows for a very good particle identification capacity. Strictly, one has to consider interactions, decays and detection in all these detectors separately. For simplicity we will neglect most of the detector substructures. We take the neutrino flux from ref. [30].

We use two data sets from two independent studies: a search for heavy neutrinos [31] and an analysis of electron neutrino CCQE [20]. The latter gives bounds on numbers of  $\gamma$ -showers and  $e$ -showers.

1. *Resolved  $e^+e^-$  pairs: 2showers.* T2K searched the resolved  $e^+$  and  $e^-$  tracks (showers) from hypothetical heavy neutrino decays inside the Time Projection Chamber (TPC) ref. [31]. In this study  $12.34 \times 10^{20}$  ( $6.29 \times 10^{20}$ ) POT in neutrino (anti-neutrino) mode were used. The selected events consist of two tracks of opposite charge originating from a vertex in a TPC, without other tracks being observed in the TPC itself or in the detector located directly upstream (including

P0D). This gives an effective detector length of 2.7 m. The invariant mass of 2-track system was restricted by  $W_{ee} < 700$  MeV and the angle between two tracks  $< 90^\circ$ . The angle between system of the tracks and the beam axis  $\cos \theta > 0.99$ .

For the indicated number of POT, the number of observed  $e^+e^-$  shower events in neutrino mode, which satisfy the selection criteria, equals  $N_{ee}^{ND\nu,obs} = 62$ . The expected number of events from the standard sources (various neutrino interactions) is  $N_{ee}^{ND,th} = 58 \pm 2.8$ . In the antineutrino mode  $N_{ee}^{ND\bar{\nu},obs} = 16$  events have been observed, while  $N_{ee}^{ND,th} = 15.1 \pm 1.6$  is expected. We sum the events from both horn modes. We neglect the small error in the theory prediction (2.8), and combine the statistical uncertainty ( $\Delta N^{stat} = 8.8$ ) with the systematic one in quadrature. For the latter we take 15% relative uncertainty on the total number of observed events which gives ( $\Delta N^{syst} = 11.7$ ) (for experiments where systematic uncertainty is not explicitly quoted, we assume the uncertainty of 15%). With this, the following upper limits on a contribution from new physics is obtained

$$N_{2sh}^{ND} < 20 \text{ (1}\sigma\text{)}, \quad 34 \text{ (2}\sigma\text{)}, \quad 49 \text{ (2}\sigma\text{)}. \quad (80)$$

Due to particle ID capacity of ND280, the selected events can be produced by the  $e^+e^-$  pair only. We take the signature factor according to eq. (78) for 3 body  $N-$  decay, and  $f_{ee-2sh} = 1$  for two body  $B-$  decay if  $m_B > 5$  MeV.

*2. Unresolved (collinear)  $e^+e^-$ : 1 shower events.* The  $\nu_e$  CCQE interactions were detected as isolated  $e$ -like events [20]. The photon background is the most important for these events. T2K studied these single photons converted into  $e^+e^-$  pairs in the FGD1.

The event selection criteria in the analysis include the following: two tracks originate from the vertex in FGD1, the energy losses in the tracks,  $dE/dx$ , are compatible with electrons. The tracks correspond to particles of opposite sign. The invariant mass is less than  $W_{ee} < 55$  MeV (the latter was imposed to ensure that  $e^+e^-$  originate from photon conversion). As signature efficiency we adopt  $\epsilon_\gamma^{ND} = 0.3$ , taken from ref. [20].

A total numbers of events of this type  $N_\gamma^{ND,obs} = 647, 182$ , and 157 were found in the analysis of the FHC data, the electron analysis of RHC data and positron analysis of RHC data correspondingly. The simulated numbers of events that originate from SM processes (CCQE neutrino-nucleon scattering, resonant pion production, deep inelastic scattering, final state interactions of hadrons produced, *etc.*) are larger:  $N_\gamma^{ND,th} = 700.97, 193.73$  and 169.31.

We combine the event numbers from FHC and the positron RHC data<sup>4</sup>. The statistical error on the combined event numbers ( $\Delta N^{stat} = 28.1$ ) and the 15% systematic error ( $\Delta N^{syst} = 118.8$ ) are summed in quadrature. This gives the upper bound on number of isolated  $\gamma$ 's from new physics

$$N_\gamma^{ND} < 58 \text{ (1}\sigma\text{)}, \quad 181 \text{ (2}\sigma\text{)}, \quad 305 \text{ (3}\sigma\text{)}. \quad (81)$$

Due to the deficit of observed signal events with respect to the prediction, the bound is stronger. Here, signature factor  $f_{\gamma-1sh}^{ND} = 1$ .

We will not use results of a dedicated search for the single photon events at T2K ND280 in ref. [22] due to low statistics.

*3. single  $e$ -shower.* In the same ND280 study of the  $\nu_e$  CCQE interactions ref. [20] total numbers of 697, 176 and 95  $e$ -like events were found in the FHC, electron RHC and positron RHC analyses. These numbers are smaller than the expected numbers from various standard neutrino interactions: 797, 175.92 and 99.99. As before, we combine the event numbers from the FHC mode

<sup>4</sup> Including also the electron analysis would add information, but we have to take the correlation of the two analyses into account to which we have no access.

and the positron RHC mode. The statistical error ( $\Delta N^{stat} = 28.3$ ) and the 15% relative systematic error ( $\Delta N^{syst} = 120.6$ ) are added in quadrature. This leads to the upper bound on number of  $e$ -like events from new physics

$$N_e^{ND} < 17 \ (1\sigma), \quad 139 \ (2\sigma), \quad 261 \ (3\sigma). \quad (82)$$

This analysis can be used to constrain scenarios with  $\xi = e$ . The  $e - \gamma$  misidentification can be important. For the reconstruction and selection efficiency for the  $e$ -like events we use  $\epsilon_{e-sh}^{ND} = 0.3$  according to ref. [20]. Notice that in the future phases of T2K ND280 can substantially improve these bounds.

### 3. MINER $\nu$ A

The MINER $\nu$ A experiment employs the Mine Injector beam line, where 120 GeV protons hit a graphine target. The produced neutrino flux has variable energy in the range (2 - 20) GeV. We use two energy samples: ME (medium energy) with the peak at  $E_\nu^{MV} = 6$  GeV, and LE (low energy) with the peak at  $E_\nu^{MV} = 4$  GeV. The flux of usual neutrinos is substantially larger than the MB flux:

$$\phi^{MV,ME} = 3 \cdot 10^{-8} \text{cm}^{-2} (\text{POT})^{-1}. \quad (83)$$

The ratio of fluxes per POT:  $\phi_\nu^{MV,ME} / \phi_\nu^{MB} = 15$ .

The experimental setup has the following sizes:  $l_p^{MV} = 675$  m,  $l^{MV} = 935$  m,  $d^{MV} = 3$  m; the target mass equals  $m^{MV} = 6.1$  tonnes. In computations we take the distance between the detector and the up-stream absorber (the dirt) to be  $b^{MV} = 10$  m.

The MINER $\nu$ A detector consists of scintillator strips, which provide 3D information on the tracks. Good particle ID allows to identify  $1e-$  from  $1\gamma-$  and  $e^+e^-$  showers using the energy loss  $dE/dx$  (along the track or in the first 4 strips). Three different samples of data were explored: (i)  $\nu e-$  scattering, (ii) CCQE  $\nu$  interactions and (iii) appearance of isolated  $\gamma$ 's.

*1. Isolated  $\gamma$  showers.* The collaboration studied showering events with the energy loss compatible with original photons in ref. [32].

For signature selection efficiency, we use the energy-averaged selection efficiency for electron showers from the  $\nu - e$  scattering analysis in ref. [33] as a proxy:  $\epsilon_\gamma^{MV} = 70\%$ . In the analysis, 1150 events were observed while 861 events are expected from SM backgrounds. The difference,  $\Delta_{SM} = 289$  events, was attributed to the diffractive  $\pi^0$  production cross section, which corresponds to  $\Delta_{SM} = 289$  events. The cross section was fit to the data and obtained as  $(0.26 \pm 0.02 \pm 0.08) \times 10^{-39} \text{cm}^2$  from which we get the relative uncertainty of  $\sim 40\%$ .

We add in quadrature the statistical error ( $\Delta N^{stat} = 33.9$  events), 15% systematic uncertainty ( $\Delta N^{syst} = 172.5$  events), and the  $\sim 40\%$  uncertainty from the fit of the diffractive  $\pi^0$  production cross section  $\Delta_{\pi^0}$  (115.8). With this we obtain the following limit on a new physics contribution to the number of isolated  $\gamma$  showers

$$N_\gamma^{MV} < 211 \ (1\sigma), \quad 421 \ (2\sigma), \quad 632 \ (3\sigma). \quad (84)$$

*2.  $e$ -like events from the  $\nu_e$  CCQE interactions.* A total number of 3204  $e$ -like events was observed, while 2931 events were expected [34]. We sum the statistical uncertainty of the observed event count using statistical error ( $\Delta^{stat} = 56.6$ ) and 15% systematic uncertainty ( $N^{syst} = 480.7$ ); added quadratically we find an upper bounds on new physics contribution

$$N_e^{MV} < 757 \ (1\sigma), \quad 1241 \ (2\sigma), \quad 1725 \ (3\sigma). \quad (85)$$



In our computations we again use the energy-averaged selection efficiency for electron showers from the  $\nu - e$  scattering analysis in ref. [33] as signature selection efficiency:  $\epsilon_{\gamma}^{MV} = 70\%$ .

3.  *$\gamma$ -like events from the  $\nu - e$  scattering analysis.* Ref. [33] analyses the  $3.43 \times 10^{20}$  POT that were collected with the low energy (LE) neutrino beam. In this analysis, electromagnetic shower candidates were selected and their  $dE/dx$  distribution was displayed prior to  $\nu - e$  analysis cuts, cf. fig. 3 of ref. [33]. From this distribution we sum the electromagnetic showers with  $dE/dx > 4.5$  (MeV/1.7cm), to obtain 171 observed photon-like events, which practically coincide with the expected 170 events. The statistical error ( $\Delta N^{stat} = 13.1$ ) and the systematic error ( $\Delta N^{syst} = 17.1$ , using 10% error according to ref. [33]) allow us to get an upper bound on single shower events

$$N_{\gamma/ee}^{MV} < 23 \ (1\sigma), \quad 45 \ (2\sigma), \quad 66 \ (3\sigma). \quad (86)$$

A similar analysis has been carried out with the medium energy (ME) data [35],  $1.16 \times 10^{21}$  POT. Following the same procedure as above, we find 1466 observed versus 1395 expected events. We add in quadrature the statistical error ( $\Delta N^{stat} = 38.3$ ) and the systematic error ( $\Delta N^{syst} = 146.6$ , using 10% error according to ref. [35]); finally we get the following upper bound on single shower events:

$$N_{\gamma/ee}^{MV} < 223 \ (1\sigma), \quad 374 \ (2\sigma), \quad 526 \ (3\sigma). \quad (87)$$

Since no photon PID cut has been employed on the here considered data the results can be applied to  $\xi = \gamma$  and collimated electron-positron pairs,  $\xi = e^+e^-$ . Our statistical analysis shows that the constraints on the allowed number of additional photon-like events are strongest when considering this dataset, hence in Section V we will not show upper bounds from Eq. (84), but instead use Eqs. (86) and (87).

Moreover, we have set the probability that a  $\xi$  is accepted as a single electromagnetic shower to one. For the signature selection efficiency we use the electron shower selection efficiency from ref. [33]:  $\epsilon_{\nu-e}^{MV} = 70\%$ .

#### 4. NOMAD

The NOMAD experiment was sourced from the SPS proton beam with energy of 450 GeV impinging on a beryllium target. It collected a total  $2.2 \times 10^{19}$  POT. The muon neutrino flux at the detector from pion decays was larger than the one in MiniBooNE, cf. e.g. ref. [36]:

$$N_{\nu_{\mu}}^{\pi} = 6.7 \cdot 10^{-7} \text{ cm}^{-2} \text{ POT}^{-1} \quad (88)$$

The parameters of the experimental setup are  $l^{NOM} = 620$  m,  $d^{NOM} = 3.7$  m, and target mass  $m^{NOM} = 3.6$  t. We assume that the distance between the detector and the up-stream absorber (dirt) is  $\Delta^{NOM} = 10$  m. The detector has a magnetic dipole field, and its components inside the field include an active target of drift chambers (DC) with a mass of 2.7 tons, a transition radiation detector (TRD), a preshower detector (PRS), and an electromagnetic calorimeter (ECAL). The TRD provides excellent electron identification efficiency  $\epsilon_e^{NOM} > 90\%$  for isolated electrons (with momenta between 1 and 50 GeV), The charged pion rejection factor is greater than  $10^3$  [37].

The collaboration performed a search for forward photons in ref. [38] to test the model from ref. [5]. Photon candidates were selected from  $e^+e^-$  pairs with invariant mass below  $W_c^{NOM} = 95$  MeV and total shower energy lower than 4 GeV. The selection efficiency (due to various cuts) was rather low:  $\epsilon_{\gamma}^{NOM} = 0.08$ . NOMAD observed  $N_{\gamma}^{NOM,obs} = 78$  events, while an expectation of  $\gamma$ 's

from standard sources (the coherent  $\pi^0$  interaction, the deep inelastic  $\nu$ - NC interactions (NC-DIS), as well as  $\nu$ -interactions occurring outside the fiducial volume where all daughter particles, except one photon, evade detection) is  $N_{\gamma}^{NOM,th} = 76.6 \pm 4.9(stat) \pm 1.9(syst)$ .

We sum quadratically the statistical error on the number of observed events ( $\Delta N^{stat} = 8.8$ ), the systematical uncertainty of 15% ( $\Delta N^{syst} = 11.7$ ), and the error from the theory prediction ( $\Delta N^{theory} = 6.8$ ) to derive an upper limit on the new physics contribution to the number of single photon events:

$$N_{\gamma/ee}^{MV} < 18 \quad (1\sigma), \quad 34 \quad (2\sigma), \quad 50 \quad (3\sigma). \quad (89)$$

This limit applies to the final states  $\xi = \gamma$  and collimated electron-positron pairs  $\xi = e^+e^-$  with invariant mass below  $W_c^{NOM}$ .

## 5. PS191

The PS191 experiment was sourced by the PS proton beam with an energy of 19.2 GeV interacting with a beryllium target and it collected  $2 \cdot 10^{19}$  POT. The  $\nu_{\mu}$  flux at the detector from pion decays was  $\phi_{\nu_{\mu}}^{\pi} = 2.3 \cdot 10^{-4} \text{ cm}^{-2}\text{POT}^{-1}$ . The setup has the following parameters:  $l^{PS} = 128$  m,  $l_p^{PS} = 49.1$  m. The detector was composed of a decay volume and a down-stream calorimeter. The decay volume of length  $d^{PS} = 12$  m was filled with flash chambers for tracking and helium bags and therefore had negligible mass. The calorimeter consisted of sandwiches made from flash chambers and 3 mm thick iron plates. Two studies have been performed.

*1. Vertices from 2 tracks in the decay volume.* Events induced by heavy neutrinos that decay in the decay volume were searched for in ref. [39]. These events should have two tracks in the decay volume and an energy deposit in the calorimeter. The vertex of the two tracks can be reconstructed. The criteria was that the reconstructed vertex should be more than 2 cm away from a flash chamber. Not a single vertex was found; this null result constrains the contribution from heavy neutrinos with decay into  $\xi$  that leaves two charged tracks in the flash chambers. The limit on events with 2 tracks reads, at 95% C.L.[39]:

$$N_{2tr}^{PS,obs} < 2.3, \quad 95\% \text{C.L.} \quad (90)$$

We apply this limit for the final states  $\xi = \gamma\gamma$  and  $\xi = e^+e^-$  with an invariant mass above the threshold  $W_c^{PS} = 30$  MeV. This threshold was derived from ref. [39], where heavy neutrinos with  $m_N \sim 30$  MeV are still subject to constraints. For the signature selection efficiency we use the signal selection efficiency from ref. [39]  $\epsilon_{2tr}^{PS} = 0.28$ .

*2. Single showers in the calorimeter.* The good granularity of the calorimeter allows to distinguish photon from electron showers. The analysis in ref. [40] studies electromagnetic showers in the calorimeter. They select events with energies above 400 MeV to reject  $\pi^0$  events and a single shower to suppress backgrounds from  $\pi^0$  decay. We use the reconstruction efficiency from ref. [39] as a proxy for the signal selection efficiency:  $\epsilon_{1sh}^{PS} = 0.7$ . Showers can be produced from  $\nu_{\mu}$  interactions, in particular from final states including  $\gamma$ ,  $\pi^0$ ,  $e$ , and from hadrons. Hadron misidentification is at most 1%. The sub-sample with an electron-likelihood selection cut yields an excess of the  $e$ -like events in the calorimeter

$$N_{1sh}^{PS,obs} = 23 \pm 8, \quad (91)$$

that was attributed to neutrino oscillations [40].

## 6. NO $\nu$ A near detector

The NO $\nu$ A experiment uses the NuMI neutrino beam sourced by interactions of 120 GeV protons with a graphite target. The parameters of setup are  $l^{NOV} = 1000$  m,  $l_p^{NOV} = 675$  m, and 14.6 mrad off line detector. The detector is a tracking calorimeter composed of fine-grained cells of liquid scintillator with a total mass of 193 t. Particle identification is based on the topological information from the tracking of particles and uses advanced pattern recognition algorithms.

*Single isolated e-shower.* The event sample corresponds to  $1.66 \cdot 10^{20}$  POT.

The analysis in ref. [41] selects neutrino interaction candidates with total energy in the range 1.5 to 2.7 GeV (the maximal  $\nu_e$  signal is expected around 2 GeV).

For the signature selection efficiency we adopt the signal selection efficiency:  $\epsilon_e^{NOV} = 33\%$ .

The observed event distribution in the calorimetric energy shows good agreement between observed  $N_e^{NOVA,obs} = 2573$  and predicted  $N_e^{NOVA,th} = 2385$ , number of events. Using statistical ( $\Delta N^{stat} = 50.7$ ) and the 15% systematic uncertainty ( $\Delta N^{syst} = 385.9$ ) we find bounds on new physics contribution:

$$N_e^{NOV} < 577 \ (1\sigma), \quad 966 \ (2\sigma), \quad 1355 \ (3\sigma). \quad (92)$$

### D. On discovery potential

Experiments we are considering are all of the same type: accelerator experiments with near or relatively close detectors. Therefore, it is straightforward to compare their discovery potentials. In various cases one can simply compare the “strengths” of experiments defined as the product of POT, efficiencies and masses of detectors:

$$\kappa^i \equiv (POT)^i \times \epsilon^i \times M^i.$$

Notice that for scenarios with decay, the active volume of a detector is important, and not a mass.

Apart from this product also other factors are important: the energy of protons and composition of a target which determine multiplicities of secondary particles, and consequently, fluxes of neutrinos. The length of baseline gives a spread of the neutrino or new particles beams, etc. Therefore, instead of (POT), one can use immediately the neutrino fluxes at detectors:

$$\kappa_\nu^i \equiv \phi_\nu^i \times \epsilon^i \times M^i,$$

or the fluxes of heavy neutrinos. The MB strength is much higher than the ND one:  $\kappa^{MB} \simeq 2 \cdot 10^{23}$  tons, while for ND280  $\kappa^{ND} = 4 \cdot 10^{21}$  tons. Using the neutrino fluxes we obtain comparable strengths:  $\kappa_\nu^{MB} = 5.4 \cdot 10^{13}$  ton cm $^{-2}$ ,  $\kappa_\nu^{ND} = 2.1 \cdot 10^{13}$  ton cm $^{-2}$ , although the MB strength is still 2.5 times larger.

Further contribution to the discovery potential comes from the particle ID. Experiments with better ID gain since a smaller subset of events can be selected, and therefore stronger bounds on new physics contributions can be obtained. This can be accounted by the ratio of the strength over the upper bound on number of events:  $\kappa_\nu^i / N^i$ . Thus, MiniBooNE has observed 638 1-shower events while ND280 upper bound is about 150. That is, ND280 gains factor of 3, and its discovery potential becomes even slightly larger than the one of MiniBooNE. Further improvements can be related to specific scenario and geometry of experiment. Thus, ND can gain in the decay scenarios because of smaller baseline. This is precisely the origin of upturns where the bound becomes stronger. To a large extent this enhancement is artificial and related to geometric suppression of number of the MB events. In upscattering scenarios sizes of detectors become important. Similarly,

Experiment	Analysis	Signature	Upper limit $1\sigma/3\sigma$	Reference
T2K ND280	Heavy neutrino decays	$e^+e^-$	20/49	[31]
	CCQE electrons	$e^- (e^+)$	17/261	[20]
	CCQE electrons	single $\gamma$	58/305	[20]
NO $\nu$ A	CCQE electrons	$e^-$	577/1355	[41]
MINER $\nu$ A	diffractive $\pi^0$ production	$\gamma$	211/632	[32]
	CCQE electrons	$e^- (e^+)$	757/1725	[34]
	Neutrino electron scattering	EM shower, or $\gamma, ee$	23/66	[33]
	Neutrino electron scattering	EM shower, or $\gamma, ee$	223/526	[35]
NOMAD	Single photon search	single $\gamma$	18/50	[38]
PS191	Heavy neutrino decays	displaced vertex	1.84/6.61	[39]
	Neutrino oscillation	electron-like events	$23 \pm 8$	[40]

TABLE I. Overview of considered experimental searches that can be used to constrain mechanisms explaining MiniBooNE.

one can consider discovery potential of other experiments and searches.

To summarize this section, we provide the salient information in Table I. In particular, the fourth row shows the upper bounds on the number of new physics events that will be confronted with theoretical predictions in Section V.

experiment	MiniBooNE	T2K	NOMAD	PS191	MINER $\nu$ A	NO $\nu$ A
area (m <sup>2</sup> )	$36\pi$	3.47	6.76	18	1.71	12.39
$\epsilon$	0.1	0.3	0.08	0.7	0.73	0.65
$d$ (m)	$2/3 \cdot 12$	$d_1 = 1, d_2 = 0.9$	3.7	3.55	3	8
$l_p$ (m)	50	94	290	49.1	675	675
POT ( $\nu + \bar{\nu}$ mode)	$3 \times 10^{21}$	$1.821 \times 10^{21}$	$2.2 \times 10^{19}$	$0.86 \times 10^{19}$	$3.43 \times 10^{20}$	$1.66 \times 10^{20}$
$M$ (tonnes)	818	$m_{P0D} = 15.8, m = 1.1$	112	20	6.1	300
$\nu$ energy range (GeV)	[0.1 – 5]	[0.1 – 10]	[5 – 200]	[0.1, 5]	[0.1 – 20]	[0.1 – 20]

TABLE II. Parameters that enter in the analysis. For T2K, we list two numbers for detector mass and its length. This is because we include the possibility that the upscattering can occur in the P0D, with the distance from TPC-FGD system that reads  $d_1 = 1$  meter.

## V. TESTS OF SCENARIOS

The bounds obtained in Section IV test the final states of different scenarios. Therefore, two different scenarios with the same final EM state have the same tests. The difference is in implications, that is, in the level of exclusion. In general, due to misidentification, any signature  $s^i$  provides bounds on all possible final states  $\xi$ , and consequently, scenarios. We call the direct test when the EM component of final state,  $\xi$ , coincides with signature: e.g.  $e - e$ -shower, etc. Indirect tests require misidentification. The most stringent bounds (best tests) are provided by the direct tests, since misidentification brings certain smallness.

Several experiments measure the same type of events (signatures) but the best bound is given by experiment which has the highest strength. These features allow to identify the relevant experimental results for each scenario.

One comment is in order.  $N$  production via  $\nu_\mu$  upscattering usually implies  $N$  mixing in  $\nu_\mu$ . Therefore, in general, for  $m_N = \mathcal{O}(100)$  MeV one has to add the contributions from  $N$  produced via mixing and upscattering mechanisms. However, these two mechanisms are effectively operative

in different ranges of  $c\tau^0$ . Namely, in upscattering case,  $N$  should decay within detector volume ( $c\tau^0 \leq 1$  m), while for the  $N$  production via mixing in the decay pipe one requires that  $N$  should reach a detector, *i.e.* survive about several hundred meters, implying  $c\tau^0 \gtrsim 100$  m.

Recall that, according to eq. (26), the predictions for all detectors are normalized to the MiniBooNE excess: the number of 1-shower events,  $N_{\xi-1sh}^{MB}$ , is proportional to  $f_{\xi-1sh}$ .

### A. Mixing - Decay scenario, $MD_\xi$

This is the simplest scenario with only two new physics interaction points: production point of  $N$  via mixing and  $N$ -decay point.  $N$  with mass  $m_N \leq 10$  MeV is produced in the  $\pi$ -decays in decay pipe and decays along the beamline.

The typical dependence of the number of events on  $c\tau^0$  (see Section III A) has the exponential upturn and approaches a constant at larger  $c\tau^0$ . The upturn point is determined by the baseline and typical energy of MiniBooNE experiment [1]. In our approximation of the signature factors being independent of  $E_N$ , such behavior is the same for all possible final states  $\xi$ .

The absolute value of excess events in a particular experiment is determined by the product (42). The final states produced in the  $N$ -decay are  $\xi = \gamma$  (radiative decay) and  $\xi = e^+e^-$  (three body decay). Also  $2\gamma$  final state can be explored, but  $\xi = e$  is not possible. Let us consider  $\xi = e^+e^-$  and  $\xi = \gamma$  in more detail.

1.  $\xi = e^+e^-$ :  $MD_{ee}$  - scenario: The  $N_{ee-2sh}^{ND}$  result (80) provides the direct test, and therefore gives the strongest bound. All other data require small invariant mass of the  $ee$  pair,  $W_{ee}$ , and imply mis-identification:  $ee$  with  $e$ -shower or  $\gamma$ -shower.

(a) For the invariant mass of the pair  $W_{ee} > W_c = 5$  MeV, the electron and positron are resolved in ND280 and therefore we can use the bound on 2e-shower events  $ND_{ee-2sh}$  (80). In Fig. 5 (left panel) we show dependence of  $N_{ee-2sh}^{ND}$  on  $c\tau^0$  for three values of mass,  $m_N$ , allowed by timing restriction [2]. In computations, we used expression (26) for  $N_{ee-2sh}^{ND}$  with parameters of experimental setup given in Table II;  $f_{ee-2sh}$  was computed using eq. (78). For the  $N$  flux at  $m_N \lesssim 10$  MeV we use active neutrino flux as a proxy.

Figure shows very strong dependence of the expected number of events on  $m_N$  which comes mainly from the signature factors. Indeed,  $N_{ee-2sh}^{ND} \propto f_{ee-2sh}^{ND}/f_{ee-1sh}^{MB}$ . In MiniBooNE, with  $W_c = 30$  MeV, the  $e^+e^-$  pairs are not resolved:  $W_{ee} < m_N < W_c$ , so that  $f_{ee-1sh}^{MB} = 1$ . In the case of ND280, the values of mass  $m_N$  are close to the threshold and therefore  $f_{ee-2sh}^{ND}$  increases strongly with  $m_N$ .

According to the figure, the scenario  $MD_{ee}$  with  $m_N > 7$  MeV is excluded. The bound relaxes with decrease of  $m_N$ , and disappears for  $m_N < 7$  MeV.

(b) For  $W_{ee} < 5$  MeV, the pair shows up in ND280 as 1sh event. This can be restricted by 1 shower searches of CCQE at ND280, as well as by PS191, NOMAD and MINERνA. Notice that this is indirect test which implies misidentification.

In Fig. 5 (right panel), we show the expected number of 1 shower events at ND280 induced by the  $e^+e^-$  pairs. The dependence of the prediction on  $m_N$  is strong but opposite to that for 2 shower events: Number of events decreases with increase of  $m_N$  again due to signature factor  $f_{ee-1sh}^{ND}$ . According to (66), for  $m_N$  above the threshold,  $f_{ee-1sh}^{ND} \propto W_c^2/m_N^2$ . (It reflects the fact that the probability of the 3-body  $N$  decay with invariant mass of the pair  $W_{ee} < W_c$  decreases.)

The opposite dependence of number of events on  $m_N$  in 1sh and 2sh cases is also reflected in the sum rule:  $f_{ee-2sh}^{ND} = 1 - f_{ee-1sh}^{ND}$ .

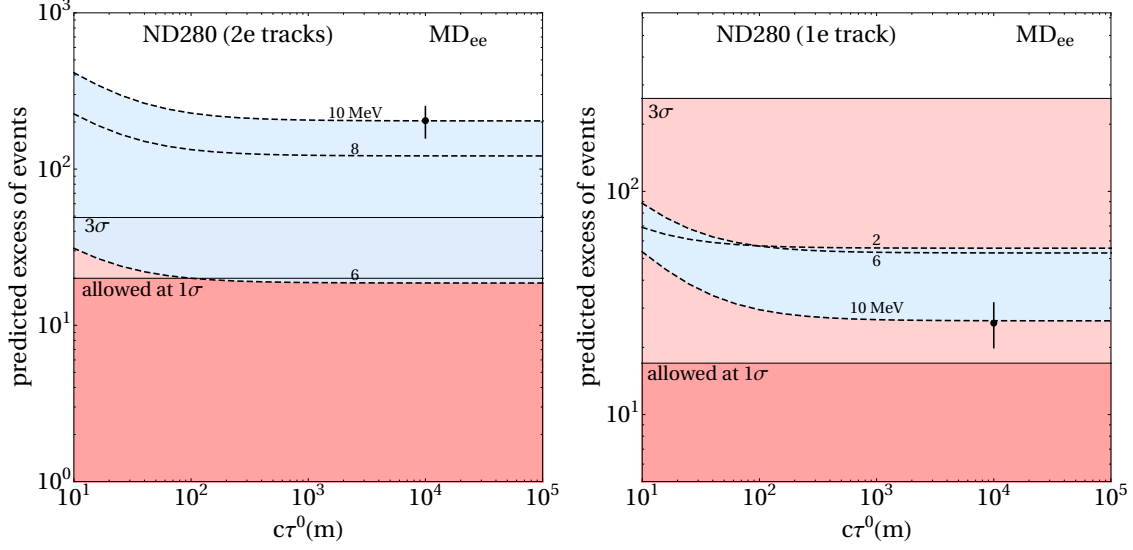


FIG. 5. Tests of the Mixing-Decay into  $e^+e^-$  scenario,  $MD_{ee}$ , at ND280. *Left panel:* Number of expected 2e-shower events produced by  $e^+e^-$  pair as function of  $c\tau^0$  for different values of  $m_N$  (numbers at the curves in MeV). The vertical section with dot shows the error for the predicted number of events. Borders of shadowed regions show the  $1\sigma$  and  $3\sigma$  experimental upper bounds on these numbers. *Right panel:* The same as in the left panel but for the 1e-shower events at ND280.

We confront our computations with the bound (82). According to Fig. 5 (right panel), the  $MD_{ee}$  scenario with  $m_N < 6$  MeV is disfavored at about  $2\sigma$  level in the whole range of  $c\tau^0$ . The bound weakens with the increase of  $m_N$ .

(c) For small  $W_{ee}$ , the final  $e^+e^-$  state can also be misidentified with  $\gamma$ -shower. In passing, we note that in such case the bounds on  $1\gamma$  shower search of new physics by NOMAD, ND280, PS191, MINERvA can also be applied (see for instance Eqs. (81) and (86)). In what follows we employ such data in order to present results of the direct test with  $\xi = \gamma$ .

2.  $\xi = \gamma$ ,  $MD_\gamma$ -scenario: The direct tests of this scenario are provided by  $1\gamma$  shower search of new physics by NOMAD (89), ND280 (81), MINERvA (84,86),

In Fig. 6 we present results for  $N$  decay into  $\gamma$  at ND280 (left) and MINERvA (right). The result for NOMAD we choose not to present as we found it not to be competitive to the tests at aforementioned two detectors. In computations, we used  $f_{1\gamma} = 1$ , and the values of  $\epsilon$  for ND280 and MINERvA can be read off from Table II (see also Section IV).

According to this figure, the predicted number of  $1\gamma$  events is at the  $1\sigma$  upper bound from ND280. Future ND280 data may improve the bound. MINERvA gives much stronger bound: For  $c\tau^0 > 10^2$  m, the prediction is at  $3\sigma$  exclusion and at  $c\tau^0 < 10^2$  m the bound becomes stronger than  $3\sigma$  especially for larger values of  $m_N$ .

The model with  $c\tau^0 \gtrsim 10^3$  m and  $m_N \sim 250$  MeV which fits this scenario (but with much bigger masses than we consider) was proposed in [6]. It is excluded by timing constraints, and independently disfavored by our consideration.



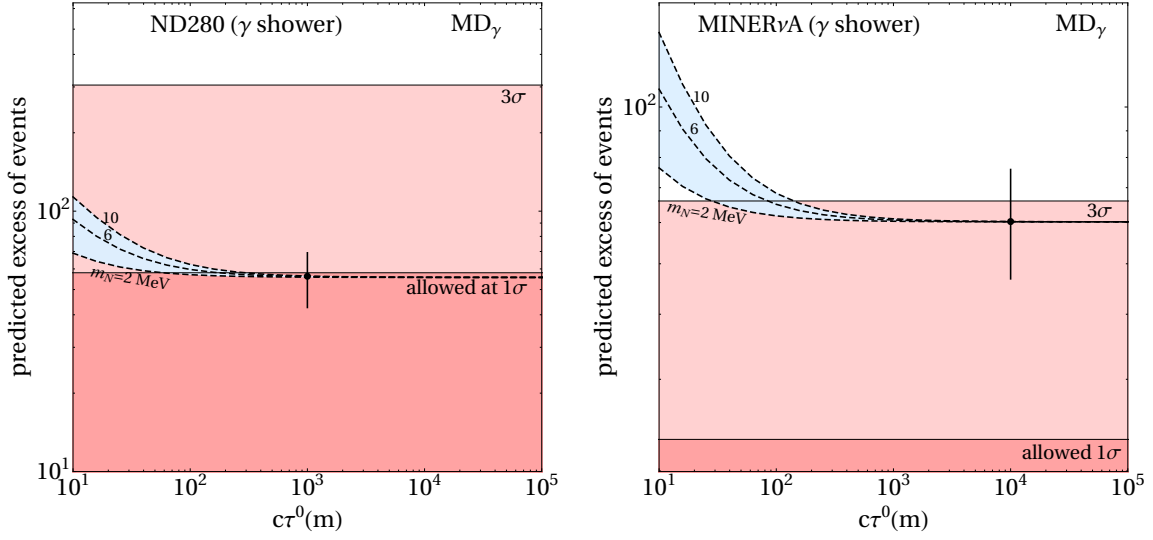


FIG. 6. Tests of the Mixing-Decay into  $\gamma$  scenario,  $MD_\gamma$ , at two different detectors. Number of expected  $\gamma$ -shower events is shown as a function of  $c\tau^0$  for different values of  $m_N$  (numbers at the curves in MeV). Borders of shadowed regions show the  $1\sigma$  and  $3\sigma$  experimental upper bounds on these numbers. *Left panel:* ND280, *Right panel:* MINERvA.

### B. Upscattering - Decay scenario, $UD_\xi$

Recall that here  $N$  is produced by  $\nu_\mu$ -upscattering in a detector as well as in matter between the decay pipe and the detector;  $N$  decays in the detector. This scenario has similar final states  $\xi$  and signatures to those of  $M_N D_\xi$ , since in both cases the final state is produced in the  $N$  decay. The difference is in geometry of  $N$ -production part, and consequently, in  $c\tau^0$  dependence, as well as in larger viable values of  $N$  mass,  $m_N \gtrsim 100$  MeV (timing constraints are much weaker in this scenario with respect to  $M_N D_\xi$ , see [2] and Section II C.)

According to Section III B, the contribution to the number of events from the  $\nu_\mu$ -upscattering in the detector has (smooth step-like) form with transition region between two asymptotics  $D^i < c\tau^0 < D^{MB}$ , where  $D^i \equiv d_i m_N / E_N$  is the reduced size of a detector. The contribution from outer matter is negligible at small  $c\tau^0$  and it increases, first linearly, then reaches maximum at  $D^i < c\tau^0$  followed by a decrease when approaching constant value in asymptotics. As we will see in the figures, the sum of the two contributions has bumpy form in the transition region.

Substantial difference from  $M_M D_\xi$  case in tests and relevance of experimental bounds is related to the masses of  $m_N$  which determine signature factors  $f$ . The latter can suppress or enhance expected numbers of events.

The final states  $\xi$  can be  $e^+e^-$  and  $\gamma$  and we will consider them in order.

#### 1. $\xi = e^+e^-$ - $U_N D_{ee}$ scenario:

ND280 data on  $e^+e^-$  pairs provide direct test of this scenario. Due to large mass of  $N$ :  $m_N \gg W_c^{ND} = 5$  MeV, the signature factor  $f_{ee-2esh}$  is close to 1.

In the left panel of Fig. 7 we show prediction for number of  $2e$ -track events,  $N_{ee-2etr}^{ND}$ , as a function of  $c\tau^0$ . Theoretical value  $N_{2e-2sh}^{ND}$  has been computed using Eqs. (26) and (52). The fluxes of  $N$  at the detector are computed using [30].

The bump at  $c\tau^0 \simeq 0.1$  m is due to contribution from the  $\nu_\mu$ -upscattering in the pion detector, P0D, in addition to TPC+FGD system. The bump is rather big since P0D has larger mass than



TPC-FGD and we consider detection in latter only. Surrounding dirt has also been taken into account; given the baseline of 280 meters and  $l_p \simeq 100$  m, the dirt extends over more than 100 meters.

The predicted number of events strongly depends on  $m_N$ . This dependence follows from the MB signature factor  $f_{ee-1sh}^{MB}$  which appears in the expression for  $N_{ee-1sh}^{MB}$  in the denominator of (26). From Eq. (78) with constant  $W_{ee}$  we have

$$f_{ee-1e}^{MB} \sim \frac{2W_c^{MB}}{m_N^2},$$

while in the numerator  $f_{ee-2e-tr}^{ND} \approx 1$ . Consequently,  $N_{ee-2etr}^{ND,obs} \propto m_N^2$ . This dependence comes from MiniBooNE instead of ND280 number of events: With increase of  $m_N$ , the decrease of  $f_{ee-1sh}^{MB}$ , should be compensated by increasing other factors in  $N_{ee-1e}^{MB}$  (e.g. coupling constants) which are also present in the expression for  $N_{2e}^{ND}$ .

Two sets of lines correspond to partially coherent  $N$  production on nuclei realized for light mediators ( $\sim 30$  MeV) and to incoherent  $N$  production due to heavy ( $> 1$  GeV) mediators (see corresponding discussion in Section IV). The difference between usage of these two types of cross sections is not large since the same type of cross section is used in numerator and denominator of Eq. (26). The mild differences appear in the intermediate region of  $c\tau^0$  where P0D and dirt also contribute.

According to the left panel of (7), the experimental bound (80) excludes the scenario in the whole range of  $c\tau^0$  and  $m_N > 50$  MeV. The model in [7] matches this scenario with  $m_N = 110$  MeV and  $c\tau^0 \gtrsim 1$  m where  $N$  is produced incoherently (mediator mass for the benchmark point is 1.25 GeV); such model appears excluded using ND280 data for 2 distinguishable  $e$  tracks (see also [42] for the independent test of this model in Icecube).

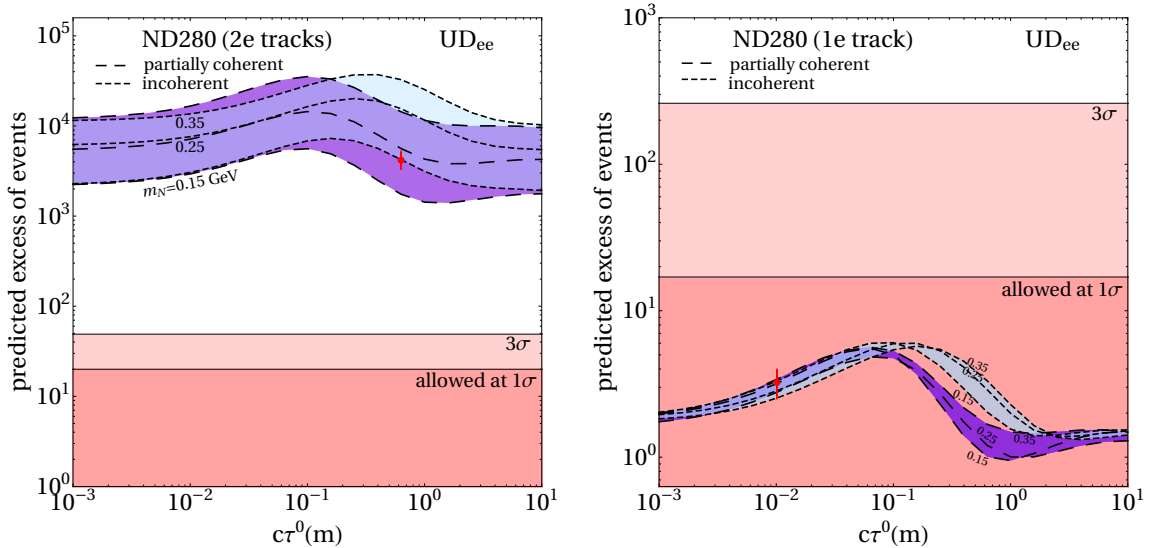


FIG. 7. Tests of (Bounds on) the Upscattering-Decay into  $e^+e^-$  scenario,  $UD_{ee}$  at ND280. *Left panel:* Number of expected 2e-track events produced by the  $e^+e^-$  pair as a function of  $c\tau^0$  for different values of  $m_N$  (numbers at the curves in GeV). The vertical section with dot shows the uncertainty in predicted number of events. Two sets of lines correspond to contributions computed with partially coherent and incoherent cross sections. The  $N$  production in dirt is taken into account. The horizontal lines show the  $1\sigma$  and  $3\sigma$  experimental upper bounds. *Right panel:* the same as in the panel a) but for the 1e-track events at ND280.

As a representative of indirect test for this scenario we use 1e-track events studied at ND280. In the right panel of Fig. 7 we show predicted excess of 1 track events induced by  $e^+e^-$  pairs at ND280. These events require very low  $W_{ee}$  and misidentification  $ee - 1$  track. The predicted number of excess events has similar dependence on  $c\tau^0$  as the one of the left side. The dependence on  $m_N$  is much weaker since the signature factors for both ND280 and MiniBooNE have the same  $1/m_N$  dependence; the signature factor enhancement is absent. Comparing to limits from Eq. (82), the predicted excess of events is below  $1\sigma$ ; hence we infer that the direct test at ND280 has much stronger power for disfavoring/excluding the class of models that have  $U_N D_{ee}$  process for the explanation of MiniBooNE anomaly.

Direct test of the  $U_N D_{ee}$  scenario can be performed using bound of the two track events from PS191 experiment (90). In the left panel of Fig. 8 we show dependence of the  $N_{ee-2tr}^{PS}$  events on  $c\tau^0$ . For this experiment we did not estimate the dirt effect; hence from both panels one may infer expected smooth step form between the asymptotics at small and large  $c\tau^0$ . Strong dependence on  $m_N$  has the same origin as in Fig. 7. Total number of events is, however, much smaller than in ND280 due to low strength of  $\kappa_\nu$  for PS191 (notice in particular low POT from Table II). Strong (more than  $3\sigma$ ) bound on the scenario appears for large masses  $m_N > 0.25$  GeV and short decay length:  $c\tau^0 < 0.1 - 1$  m.

In the right panel of Fig. 8 we show prediction for the number of 1 shower events originated from  $e^+e^-$  pair. This requires low threshold  $W_{ee} < W_c^{PS} = 30$  MeV and misidentification. According to Fig. 8, the  $U_N D_{ee}$  scenario could explain the observed excess of events at PS191. However, the required values of parameters are already excluded at more than  $3\sigma$  by two track events at ND280 (see Fig. 7).

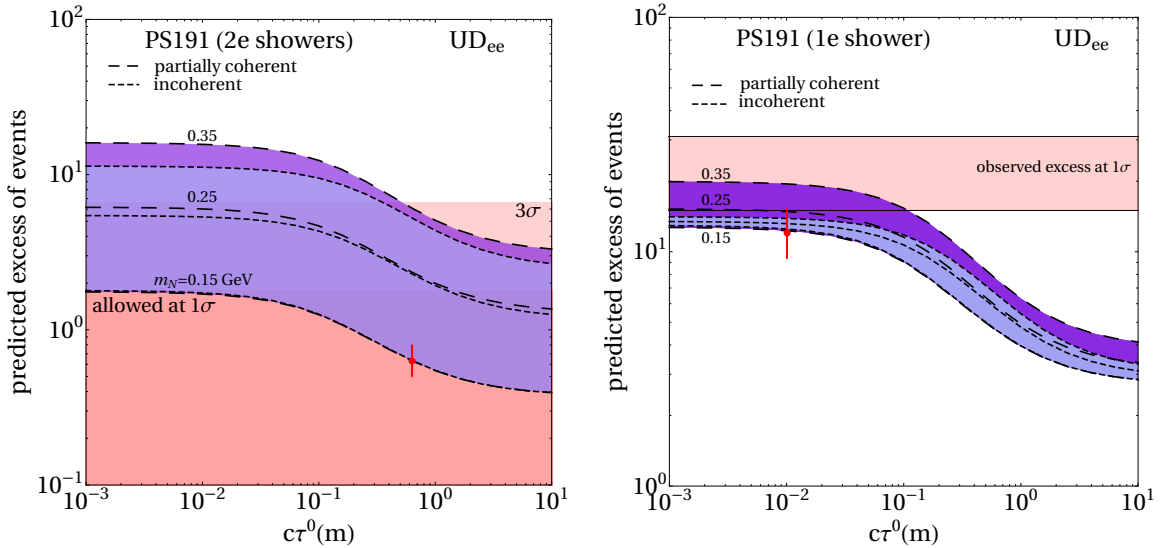


FIG. 8. The same as in Fig. 7 but at PS191.

2.  $\xi = \gamma$ :  $U_N D_\gamma$  scenario: It can be directly tested at several detectors and in particular at MINER $\nu$ A and ND280. In the left panel of Fig. 9, the number of isolated  $\gamma$  events in MINER $\nu$ A  $N_{\gamma-\gamma sh}^{MV}$  is shown as a function of  $c\tau^0$ . Both contributions from upscattering in the detector and in the dirt are included; the latter induces a bump at  $c\tau^0 = 1 - 5$  m depending on the value of  $m_N$  (if there was no dirt effect included, the shape would qualitatively resemble Fig. 8). Both in MINER $\nu$ A and MiniBooNE the signature factors for this channel are close to 1 and strong

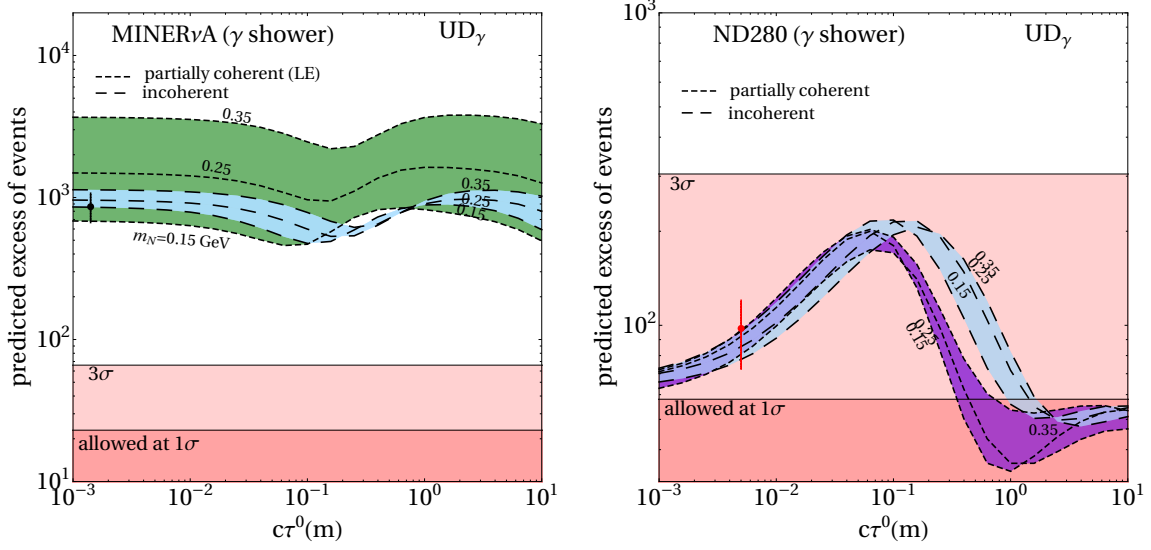


FIG. 9. Direct Tests of (Bounds on) the Upscattering-Decay into  $\gamma$ - scenario,  $UD_\gamma$  by different experiments. Number of expected  $\gamma$ -shower events as function of  $c\tau^0$  for different values of  $m_N$  (numbers at the curves in GeV) is shown. Horizontal lines show the  $1\sigma$  and  $3\sigma$  experimental upper bounds on these numbers. The vertical section shows the uncertainty in predicted number of events. Two sets of lines correspond to contributions computed with partially coherent and incoherent cross-sections. The left panel is for MINERvA while the right one corresponds to ND280.

dependence of  $N_{\gamma-\gamma sh}^{MV}$  on  $m_N$  follows from coherent cross-section: We observe that, with the increase of  $m_N$ , the cross section for partially coherent scattering drops more strongly around the typical MiniBooNE energy  $E_N^{MB} \sim 0.8$  GeV, while for MINERvA with  $E_N^{MV} \sim 5$  GeV the decrease is much weaker

$$N_{\gamma-\gamma sh}^{MV} \propto \frac{\sigma^{coh}(E_N^{MV}, m_N)}{\sigma^{coh}(E_N^{MB}, m_N)}. \quad (93)$$

As a result,  $N_{\gamma-\gamma sh}^{MV}$  increases with  $m_N$ . In the case of incoherent  $N$ -production, the dependence of the cross section on  $m_N$ , being related to integration over the phase space, is weak.

According to the left panel of Fig. 9, experimental result (86) excludes present scenario in whole range of  $c\tau^0$  and  $m_N > 0.1$  GeV. The model [5] fits this scenario with  $c\tau^0 = 0.1$  m and  $m_N \sim 0.5$  GeV, and is clearly excluded by MINERvA data.

In the right panel of Fig. 9, we show the excess of single  $\gamma$  events at ND280. The dependence has typical bump due to P0D contribution; here, the dependence of the excess on  $m_N$  is weak since now  $E_N^{MB} \approx E_N^{ND}$ . The model is disfavored at  $1-2\sigma$  level, but in future with much higher statistics the test can be significantly improved.

### C. Upscattering - Double Decay scenario, $UD_B D_\xi$

In this scenario,  $N$ , produced via the  $\nu_\mu$ -upscattering in a detector and surrounding materials, decays into on-shell boson  $N \rightarrow B + \nu$ , which in turn decays into the pair  $B \rightarrow e^+ e^-$ . Alternatively,  $B$  can undergo a radiative decay  $B \rightarrow B' + \gamma$ .  $B$  (as well as  $B'$ ) can be new vector ( $Z'$ ) or scalar ( $\phi$ ) boson. Notice, in this double decay scenario there are three vertices with new physics interactions:  $N$ -production,  $N$ -decay and  $B$ -decay.

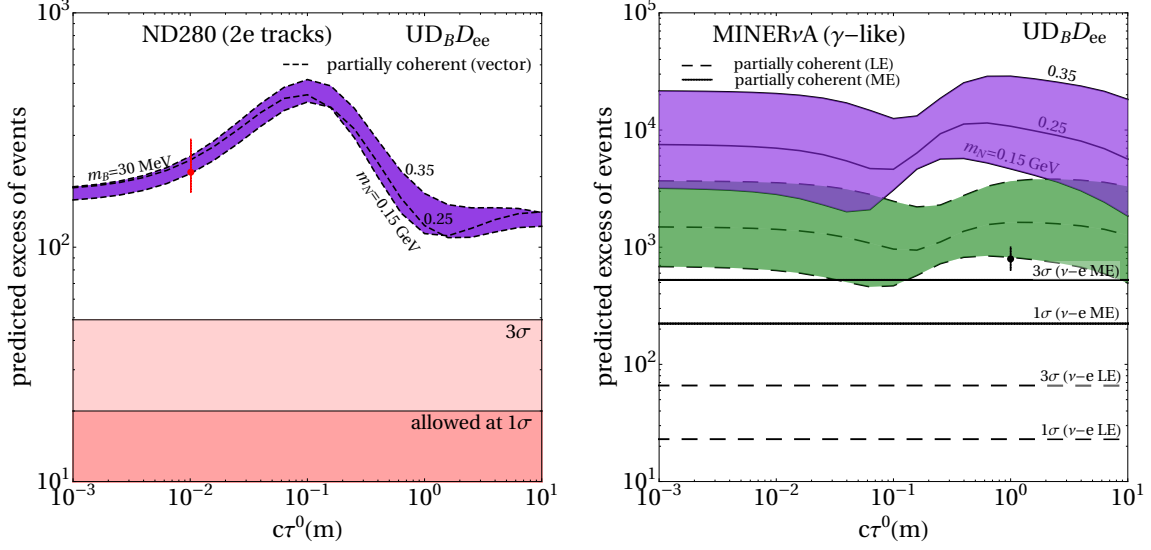


FIG. 10. Tests of the Upscattering-Double Decay into  $e^+e^-$  scenario,  $UD_B D_{ee}$  at ND280 (left) and MINERνA (right). *Left panel:* Number of expected 2e-track events produced by the  $e^+e^-$  pair at ND280 as a function of  $c\tau^0$  for different values of  $m_N$  (numbers at the curves in GeV). We take  $m_B = 30$  MeV. The horizontal lines show the  $1\sigma$  and  $3\sigma$  experimental upper bounds on the 2e-track events. The vertical section shows the uncertainty in predicted number of events. *Right panel:* Number of expected  $\gamma$ -like shower events at MINERνA as a function of  $c\tau^0$  for different values of  $m_N$  (numbers at the curves in GeV). We take  $m_B = 30$  MeV. Two sets of lines correspond to contribution of the ME and LE samples of events. Partially coherent cross-section was used.

If  $B$  decays fast, so that the decay length is smaller or comparable to the size of the detector, effectively the picture of transitions will be similar to that of  $UD_\xi$  scenario. Correspondingly, time development, signatures and relevant experiments will be similar. The only difference is that in the  $\xi = e^+e^-$  case the invariant mass of the pair is fixed by the mass of  $B$ ,  $W_{ee} = m_B$ .

In what follows we will consider the case  $\xi = e^+e^-$ , that is, the  $U_N D_B D_{ee}$ -scenario while assuming fast  $B$  decay.

If  $m_B > W_c^{ND} = 5$  MeV, the ND280 can provide a direct test of this scenario and therefore give the most stringent bound.

The dependence of number of events,  $N_{ee-2sh}^{ND}$ , on  $c\tau^0$ , shown in the left panel of Fig. 10, has typical dependence with two flat asymptotics and bump at about 0.1 m due to  $N$  production in the outer P0D detector. (It is similar to dependence in Fig. 7 (left) and Fig. 9 (right)). In computations, we use partially coherent cross section. Dependence on  $m_N$  is rather weak. The signature factor enhancement is absent for  $m_B \leq W_c^{MB} = 30$  MeV; MiniBooNE does not resolve the pair and therefore  $f_{ee-1sh}^{MB} \approx 1$ . On the other hand, for  $m_B \gg W_c^{ND}$ , we have  $f_{ee-2sh}^{ND} \approx 1$ . For larger  $m_B$ , one would expect suppression of  $f_{ee-1sh}^{MB}$ , and consequently further signature factor enhancement of the number of events. Still, there is a weak dependence on  $m_N$  due to partially coherent cross section dependence and slightly higher effective energy of ND280 than that of MiniBooNE. The reason is the same as for MINERνA test of  $U_N D_\gamma$  scenario described in Section VB.

The experimental bounds in Eq. (80) (the same as in Fig. 7 left), exclude this scenario at more than  $3\sigma$  CL in the whole range of  $c\tau^0$  and  $m_B > 10$  MeV. With further decrease of  $m_B$  (approaching  $W_c^{ND}$ ) the number of events is suppressed by the signature factor. For  $m_B < 5$  MeV, the ND280 bound on 2 shower events is not applicable, but one can use various indirect tests instead.

Strong indirect test of the  $U_N D_B D_{ee}$ -scenario, which requires the  $ee - \gamma$  shower misidentification, can be performed with MINER $\nu$ A  $\gamma$ -shower bounds (86).

In Fig. 10 (right panel), we show predictions for the number of  $\gamma$ -like shower events at MINER $\nu$ A. The dependence of  $N_{ee-\gamma}^{MV}$  on  $c\tau^0$  has typical smooth step form with the bump due to dirt effect. The bump is at larger decay length than in other experiments,  $c\tau^0 = 0.5 - 3$  m due to larger distance between the detector and the outer material. The purple and green regions correspond to ME and LE MINER $\nu$ A datasets. Strong dependence of the number of events on  $m_N$  is due to the coherent cross section enhancement, as explained around Eq. (93).

Much stronger effect than in the left panel is related to higher neutrino energies at MINER $\nu$ A and therefore weaker suppression of the cross-section with increase of  $m_N$ , than at ND280 and MiniBooNE. For this reason, the prediction for ME sample is higher than for LE sample (in addition, ME dataset comes with  $\sim 3$  more POT). The signature factor enhancement is absent here.

The predictions are much higher than the upper bounds on  $\gamma$ -shower events given in Eqs. (86) and (87). The LE sample provides stronger bound than ME one.

The scenario is excluded at more than  $3\sigma$  level in the whole range of  $c\tau^0$  and  $m_N > 0.1$  MeV. This is in agreement with the results of the detailed analysis performed in ref. [43].

The model [9] matches this scenario for  $c\tau^0 = \mathcal{O}(10^{-9})$  cm,  $m_B = 30$  MeV and  $m_N \sim 0.25$  GeV, and is consequently disfavored both by ND280 and MINER $\nu$ A.

#### D. Mixing - Decay into $\nu_e$ scenario, $MD_\nu$

In this scenario,  $N$  is produced via mixing in  $\nu_\mu$ , then  $N$  decays along the beamline into  $\nu_e$ ,  $N \rightarrow \nu_e + B$ , and in turn,  $\nu_e$  upscatters in a detector producing  $e$ -like events in the low energy range (if  $B$  has large enough mass). In this way an additional  $\nu_e$  flux is generated.

The direct tests of this scenario are provided by studies of  $e$ -like events at ND280, MINER $\nu$ A, PS191 and NO $\nu$ A (Fig. 11). The numbers of events due to  $MD_\nu$  scenario in these experiments,  $N_{e-esh}^i$ , have been computed using Eqs. (68) and (69). According to analysis in Section III D, these  $N_{e-esh}^i$  as functions of  $c\tau^0$  have smooth step-like form with constant asymptotics at  $c\tau^0 \rightarrow 0$  and  $c\tau^0 \rightarrow \infty$  (see Eq. (75)), and with transition region at

$$c\tau^{0i} \sim l^i \frac{m_N}{E^i}. \quad (94)$$

Here,  $l^i$  is the baseline. The asymptotics do not depend on  $m_N$ , and transition region shifts with  $m_N$ , proportionally to  $m_N$ .

The limits for a single electron shower are given in Eqs. (82), (85), (89) and (91). For MINER $\nu$ A, the predicted number of events is well below the  $1\sigma$  limit. Prediction of ND280 is slightly above  $1\sigma$ , while, interestingly, the calculated event number at PS191 is almost consistent with previously observed excess at that experiment (Section IV). NO $\nu$ A is disfavoring this scenario at the level of  $1\sigma$  at large  $c\tau^0$ , and at the level of  $3\sigma$  at small  $c\tau^0$ . Notice that NO $\nu$ A already collected much more data with respect to the analysis given in [41] on which our limits are based. Therefore an updated analysis can further improve the bounds.

The models [13, 14] realize this scenario with  $c\tau^0 \sim 10^{-3}$  cm and  $m_M = 1 - 10$  keV. Therefore, with present data they are disfavored at about  $3\sigma$ .

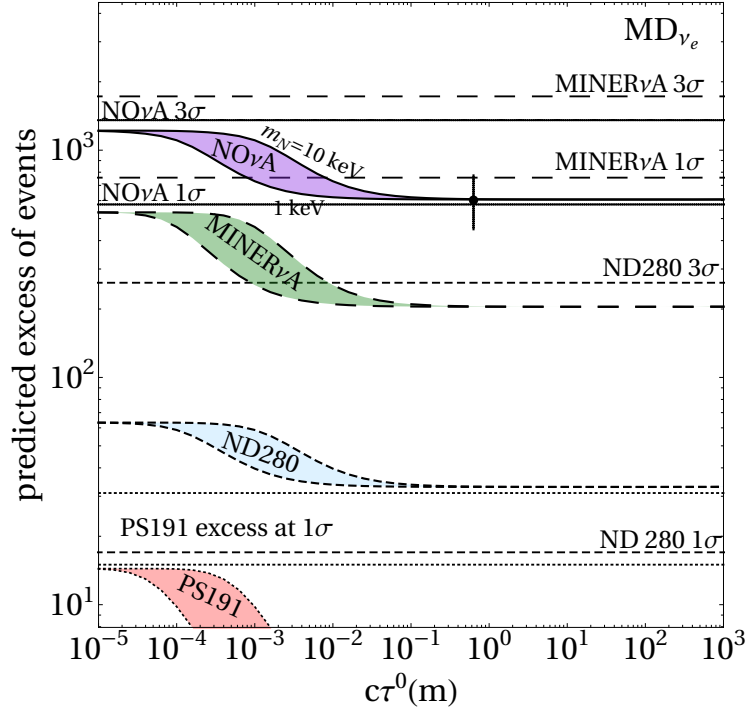


FIG. 11. Direct Tests of the Mixing - Decay into  $\nu_e$  scenario,  $MD_{\nu}$ . Number of expected events as a function of  $c\tau^0$  for different values of  $m_N$  (numbers at the curves in keV) are shown for ND280, MINER $\nu$ A, PS191 and NO $\nu$ A. Horizontal lines correspond to the  $1\sigma$  and  $3\sigma$  experimental upper bounds for each of these experiments. The vertical section shows the uncertainty in predicted number of events.

## VI. SUMMARY AND CONCLUSIONS

We performed a model independent study of the non-oscillatory explanations of the MiniBooNE excess in terms of the phenomenological scenarios. The latter are series of transitions and processes which connect initial interactions of the accelerated protons with target and appearance of single shower ( $e$ -like) events in the MiniBooNE detector. The processes include production of new particles and their decays as well as their propagation and interactions with medium. We parametrized scenarios by masses and decay rates of new particles as well as cross sections.

We carried out systematic search of the simplest scenarios which can be classified by the number of new interaction points (vertices). We have found 2 scenarios with 2 vertices, 4 scenarios with 3 vertices, etc. More possibilities are related to the nature of new propagating particles (fermions or bosons) as well as to the type of particle(s) in the final state which produce single shower events in MiniBooNE. We show that these scenarios are reduced to four qualitatively different configurations.

For these configurations, general formulas have been derived for the number of events due to new physics. Dependence of the number of events on parameters of scenarios were considered. In particular, we find three qualitatively different dependences on  $c\tau^0$ : flat dependence with upturn at small  $c\tau^0$  (scenarios with mixing), smooth step-like dependence (scenarios with upscattering in detector), bump followed by constant in large  $c\tau^0$  asymptotics (scenarios with upscattering in dirt). In a sense, we developed effective theory of new physics at the low energy accelerator experiments.



We described tests of the scenarios employing neutrino experiments which have setups similar to the MiniBooNE one: experiments at near detectors of NO $\nu$ A and T2K (ND280) as well as at PS191, MINER $\nu$ A and NOMAD. While reproducing MiniBooNE excess, the scenarios lead to additional events in these experiments. In other words, scenarios allow to directly connect the observed MiniBooNE excess of events to expected excesses in other experiments. In practice, we normalize the expected number of events in a given experiment to the MiniBooNE excess, and in this way various parameters and uncertainties cancel out.

For each experiment under consideration we obtained the upper bounds on possible numbers of events due to new physics. We confronted these bounds with expected number of events related to MiniBooNE excess.

We find that in spite of large strength of MiniBooNE (mass, POT) other experiments produce substantial bounds due to better particle ID, higher neutrino energies, dependence of cross-section on mass of produced particle, etc. In particular, we find the significance factor enhancement and coherent cross section enhancement.

We find that all scenarios are either excluded or disfavored by the data from at least one considered experiment. In particular,  $U_N D_{ee}$  and  $U_N D_B U_{ee}$  scenarios are excluded by the 2e-tracks data from ND280.  $UD_\gamma$  is excluded by data on isolated photons from MINER $\nu$ A. As far as the MD scenarios with  $m_N < 10$  MeV are concerned, they are disfavored by ND280 2e-tracks (higher masses are already excluded by MiniBooNE timing data). The  $MD_\nu$  scenario should have already produced significant excess of events at NO $\nu$ A with the present tension at  $3\sigma$  level.

We hence conclude that the MiniBooNE anomaly is likely not induced by new physics effects but rather stems from underestimating the backgrounds.

## ACKNOWLEDGEMENTS

OF would like to thank Bill Louis for fruitful email correspondence. VB would like to thank Sumit Ghosh and Joachim Kopp for useful discussions.

- 
- [1] **MiniBooNE** Collaboration, A. A. Aguilar-Arevalo et al., *Significant Excess of ElectronLike Events in the MiniBooNE Short-Baseline Neutrino Experiment*, *Phys. Rev. Lett.* **121** (2018), no. 22 221801, [[arXiv:1805.12028](#)].
  - [2] **MiniBooNE** Collaboration, A. Aguilar-Arevalo et al., *Updated MiniBooNE Neutrino Oscillation Results with Increased Data and New Background Studies*, [arXiv:2006.16883](#).
  - [3] J. Asaadi, E. Church, R. Guenette, B. J. P. Jones, and A. M. Szelc, *New light Higgs boson and short-baseline neutrino anomalies*, *Phys. Rev.* **D97** (2018), no. 7 075021, [[arXiv:1712.08019](#)].
  - [4] M. Dentler, A. Hernández-Cabezudo, J. Kopp, P. A. Machado, M. Maltoni, I. Martinez-Soler, and T. Schwetz, *Updated Global Analysis of Neutrino Oscillations in the Presence of eV-Scale Sterile Neutrinos*, *JHEP* **08** (2018) 010, [[arXiv:1803.10661](#)].
  - [5] S. N. Gninenko, *The MiniBooNE anomaly and heavy neutrino decay*, *Phys. Rev. Lett.* **103** (2009) 241802, [[arXiv:0902.3802](#)].
  - [6] O. Fischer, A. Hernández-Cabezudo, and T. Schwetz, *Explaining the MiniBooNE excess by a decaying sterile neutrino with mass in the 250 MeV range*, [arXiv:1909.09561](#).
  - [7] P. Ballett, S. Pascoli, and M. Ross-Lonergan,  *$U(1)'$  mediated decays of heavy sterile neutrinos in MiniBooNE*, *Phys. Rev.* **D99** (2019) 071701, [[arXiv:1808.02915](#)].
  - [8] A. Abdullahi, M. Hostert, and S. Pascoli, *A Dark Seesaw Solution to Low Energy Anomalies: MiniBooNE, the muon ( $g-2$ ), and BaBar*, [arXiv:2007.11813](#).



- [9] E. Bertuzzo, S. Jana, P. A. N. Machado, and R. Zukanovich Funchal, *Dark Neutrino Portal to Explain MiniBooNE excess*, *Phys. Rev. Lett.* **121** (2018), no. 24 241801, [[arXiv:1807.09877](#)].
- [10] A. Datta, S. Kamali, and D. Marfatia, *Dark sector origin of the KOTO and MiniBooNE anomalies*, *Phys. Lett. B* **807** (2020) 135579, [[arXiv:2005.08920](#)].
- [11] B. Dutta, S. Ghosh, and T. Li, *Explaining  $(g - 2)_{\mu,e}$ , KOTO anomaly and MiniBooNE excess in an extended Higgs model with sterile neutrinos*, [arXiv:2006.01319](#).
- [12] W. Abdallah, R. Gandhi, and S. Roy, *Understanding the MiniBooNE and the muon  $g - 2$  anomalies with a light  $Z'$  and a second Higgs doublet*, [arXiv:2006.01948](#).
- [13] A. de Gouvêa, O. L. G. Peres, S. Prakash, and G. V. Stenico, *On The Decaying-Sterile Neutrino Solution to the Electron (Anti)Neutrino Appearance Anomalies*, [arXiv:1911.01447](#).
- [14] M. Dentler, I. Esteban, J. Kopp, and P. Machado, *Decaying Sterile Neutrinos and the Short Baseline Oscillation Anomalies*, [arXiv:1911.01427](#).
- [15] Y. Bai, R. Lu, S. Lu, J. Salvado, and B. A. Stefanek, *Three Twin Neutrinos: Evidence from LSND and MiniBooNE*, *Phys. Rev. D* **93** (2016), no. 7 073004, [[arXiv:1512.05357](#)].
- [16] T. Katori, V. Kostelecky, and R. Tayloe, *Global three-parameter model for neutrino oscillations using Lorentz violation*, *Phys. Rev. D* **74** (2006) 105009, [[hep-ph/0606154](#)].
- [17] Y. Farzan, T. Schwetz, and A. Y. Smirnov, *Reconciling results of LSND, MiniBooNE and other experiments with soft decoherence*, *JHEP* **07** (2008) 067, [[arXiv:0805.2098](#)].
- [18] **MiniBooNE DM** Collaboration, A. Aguilar-Arevalo et al., *Dark Matter Search in Nucleon, Pion, and Electron Channels from a Proton Beam Dump with MiniBooNE*, *Phys. Rev. D* **98** (2018), no. 11 112004, [[arXiv:1807.06137](#)].
- [19] J. R. Jordan, Y. Kahn, G. Krnjaic, M. Moschella, and J. Spitz, *Severe Constraints on New Physics Explanations of the MiniBooNE Excess*, *Phys. Rev. Lett.* **122** (2019), no. 8 081801, [[arXiv:1810.07185](#)].
- [20] **T2K** Collaboration, K. Abe et al., *Measurement of the charged-current electron (anti-)neutrino inclusive cross-sections at the T2K off-axis near detector ND280*, [arXiv:2002.11986](#).
- [21] p. c. Bill Louis.
- [22] **T2K** Collaboration, K. Abe et al., *Search for neutral-current induced single photon production at the ND280 near detector in T2K*, *J. Phys. G* **46** (2019), no. 8 08LT01, [[arXiv:1902.03848](#)].
- [23] D. Kim, P. A. Machado, J.-C. Park, and S. Shin, *Optimizing Energetic Light Dark Matter Searches in Dark Matter and Neutrino Experiments*, *JHEP* **07** (2020) 057, [[arXiv:2003.07369](#)].
- [24] J. A. Formaggio and G. P. Zeller, *From eV to EeV: Neutrino Cross Sections Across Energy Scales*, *Rev. Mod. Phys.* **84** (2012) 1307–1341, [[arXiv:1305.7513](#)].
- [25] **MiniBooNE** Collaboration, A. A. Aguilar-Arevalo et al., *The Neutrino Flux prediction at MiniBooNE*, *Phys. Rev.* **D79** (2009) 072002, [[arXiv:0806.1449](#)].
- [26] **T2K** Collaboration, K. Abe et al., *The T2K Experiment*, *Nucl. Instrum. Meth.* **A659** (2011) 106–135, [[arXiv:1106.1238](#)].
- [27] **T2K** Collaboration, Y. Kudenko, *The Near neutrino detector for the T2K experiment*, *Nucl. Instrum. Meth.* **A598** (2009) 289–295, [[arXiv:0805.0411](#)].
- [28] S. Assylbekov et al., *The T2K ND280 Off-Axis Pi-Zero Detector*, *Nucl. Instrum. Meth. A* **686** (2012) 48–63, [[arXiv:1111.5030](#)].
- [29] **T2K ND280 FGD** Collaboration, P. Amaudruz et al., *The T2K Fine-Grained Detectors*, *Nucl. Instrum. Meth. A* **696** (2012) 1–31, [[arXiv:1204.3666](#)].
- [30] **T2K** Collaboration, K. Abe et al., *T2K neutrino flux prediction*, *Phys. Rev.* **D87** (2013), no. 1 012001, [[arXiv:1211.0469](#)]. [Addendum: *Phys. Rev.* **D87**, no. 1, 019902 (2013)].
- [31] **T2K** Collaboration, K. Abe et al., *Search for heavy neutrinos with the T2K near detector ND280*, *Phys. Rev.* **D100** (2019), no. 5 052006, [[arXiv:1902.07598](#)].
- [32] **MINERvA** Collaboration, J. Wolcott et al., *Evidence for Neutral-Current Diffractive  $\pi^0$  Production from Hydrogen in Neutrino Interactions on Hydrocarbon*, *Phys. Rev. Lett.* **117** (2016), no. 11 111801, [[arXiv:1604.01728](#)].
- [33] **MINERvA** Collaboration, J. Park et al., *Measurement of Neutrino Flux from Neutrino-Electron Elastic Scattering*, *Phys. Rev.* **D93** (2016), no. 11 112007, [[arXiv:1512.07699](#)].
- [34] **MINERvA** Collaboration, J. Wolcott et al., *Measurement of electron neutrino quasielastic and quasielasticlike scattering on hydrocarbon at  $\langle E_\nu \rangle = 3.6$  GeV*, *Phys. Rev. Lett.* **116** (2016), no. 8 081802, [[arXiv:1509.05729](#)].

- [35] **MINERvA** Collaboration, E. Valencia et al., *Constraint of the MINERvA medium energy neutrino flux using neutrino-electron elastic scattering*, *Phys. Rev.* **D100** (2019), no. 9 092001, [[arXiv:1906.00111](#)].
- [36] F. Vannucci, *The NOMAD Experiment at CERN*, *Adv. High Energy Phys.* **2014** (2014) 129694.
- [37] **NOMAD** Collaboration, P. Astier et al., *Search for heavy neutrinos mixing with tau neutrinos*, *Phys. Lett. B* **506** (2001) 27–38, [[hep-ex/0101041](#)].
- [38] **NOMAD** Collaboration, C. T. Kullenberg et al., *A search for single photon events in neutrino interactions*, *Phys. Lett.* **B706** (2012) 268–275, [[arXiv:1111.3713](#)].
- [39] G. Bernardi et al., *FURTHER LIMITS ON HEAVY NEUTRINO COUPLINGS*, *Phys. Lett.* **B203** (1988) 332–334.
- [40] G. Bernardi, G. Carugno, J. Chauveau, F. Di Carlo, M. Dris, J. Dumarchez, M. Ferro-Luzzi, J. M. Lvy, D. Lukas, J. M. Perreau, Y. Pons, A. M. Touchard, and F. Vannucci, *Anomalous electron production observed in the CERN PS neutrino beam*, *Phys. Lett. B* **181** (May, 1986) 173–177. 11 p.
- [41] **NOvA** Collaboration, P. Adamson et al., *First measurement of electron neutrino appearance in NOvA*, *Phys. Rev. Lett.* **116** (2016), no. 15 151806, [[arXiv:1601.05022](#)].
- [42] P. Coloma, *Icecube/DeepCore tests for novel explanations of the MiniBooNE anomaly*, *Eur. Phys. J.* **C79** (2019), no. 9 748, [[arXiv:1906.02106](#)].
- [43] C. A. Argelles, M. Hostert, and Y.-D. Tsai, *Testing New Physics Explanations of MiniBooNE Anomaly at Neutrino Scattering Experiments*, *Phys. Rev. Lett.* **123** (2019), no. 26 261801, [[arXiv:1812.08768](#)].